MNRAS **477,** 5191–5206 (2018)
Advance Access publication 2018 April 19

doi:10.1093/mnras/sty949

Circumstellar disc lifetimes in numerous galactic young stellar clusters

A. J. W. Richert,[1] K. V. Getman,[1]★ E. D. Feigelson,[1] M. A. Kuhn,[2,3] P. S. Broos,[1] M. S. Povich,[4] M. R. Bate[5] and G. P. Garmire[6]

[1]*Department of Astronomy & Astrophysics, 525 Davey Laboratory, Pennsylvania State University, University Park, PA 16802, USA*
[2]*Instituto de Fisica y Astronomia, Universidad de Valparaiso, Gran Bretana 1111, 2360102 Playa Ancha, Valparaiso, Chile*
[3]*Millenium Institute of Astrophysics, Av. Vicuna Mackenna 4860, 782-0436 Macul, Santiago, Chile*
[4]*Department of Physics and Astronomy, California State Polytechnic University, 3801 West Temple Ave, Pomona, CA 91768, USA*
[5]*Department of Physics and Astronomy, University of Exeter, Stocker Road, Exeter, Devon EX4 4QL, UK*
[6]*Huntingdon Institute for X-ray Astronomy, LLC, 10677 Franks Road, Huntingdon, PA 16652, USA*

Accepted 2018 April 11. Received 2018 March 23; in original form 2017 December 31

ABSTRACT

Photometric detections of dust circumstellar discs around pre-main sequence (PMS) stars, coupled with estimates of stellar ages, provide constraints on the time available for planet formation. Most previous studies on disc longevity, starting with Haisch, Lada & Lada, use star samples from PMS clusters but do not consider data sets with homogeneous photometric sensitivities and/or ages placed on a uniform time-scale. Here we conduct the largest study to date of the longevity of inner dust discs using X-ray and 1–8 μm infrared photometry from the MYStIX and SFiNCs projects for 69 young clusters in 32 nearby star-forming regions with ages $t \leq 5$ Myr. Cluster ages are derived by combining the empirical Age_{JX} method with PMS evolutionary models, which treat dynamo-generated magnetic fields in different ways. Leveraging X-ray data to identify disc-free objects, we impose similar stellar mass sensitivity limits for disc-bearing and disc-free young stellar objects while extending the analysis to stellar masses as low as $M \sim 0.1$ M$_\odot$. We find that the disc longevity estimates are strongly affected by the choice of PMS evolutionary model. Assuming a disc fraction of 100 per cent at zero age, the inferred disc half-life changes significantly, from $t_{1/2} \sim 1.3$–2 Myr to $t_{1/2} \sim 3.5$ Myr when switching from non-magnetic to magnetic PMS models. In addition, we find no statistically significant evidence that disc fraction varies with stellar mass within the first few Myr of life for stars with masses <2 M$_\odot$, but our samples may not be complete for more massive stars. The effects of initial disc fraction and star-forming environment are also explored.

Key words: stars: early-type – stars: formation – stars: pre-main sequence – open clusters and associations: general – infrared: stars – X-rays: stars.

1 INTRODUCTION

The time required to assemble planets in young circumstellar discs remains a key variable in planet formation theory. Given that planets form out of gas and dust in young circumstellar discs following protostellar collapse, observed lifetimes of the gas and dust phases translate into constraints on the time available to form Jovian and terrestrial planets, respectively (Youdin & Goodman 2005; Lyra et al. 2008; Boss 2010). Measuring disc lifetimes also play a role in constraining models of disc evolution more generally, as disc material is depleted by accretion on to the star, internal and external photoevaporation, disc winds, and planetesimal and planet formation (Lynden-Bell & Pringle 1974; Pringle 1981; Bell et al. 1997; Armitage 2011; Bai 2011; Königl & Salmeron 2011). Since disc evolution may be dominated by turbulent viscosity, observationally derived disc lifetimes are often used to estimate characteristic viscous α values (Shakura & Sunyaev 1973).

Alpha-disc theory allows a disc to be long-lived or short-lived depending on the unknown viscosity (Armitage 2011), therefore in the absence of robust theoretical constraints on effective α values, the actual distribution of longevities for an ensemble of discs must be evaluated observationally. In principle, initial disc masses and disc depletion rates for individual systems could be used to estimate disc lifetimes, however initial disc masses cannot be retrospectively determined for individual systems, and there is no reason to assume that disc dissipation rates are constant over the long lifetime of a disc. In fact, there is strong evidence that accretion rates are fast during the protostellar phase and slow during later pre-main sequence (PMS) phases, and may be variable on shorter time-scales

★ E-mail: gkosta@astro.psu.edu

as well (Bouvier et al. 1993; Alencar et al. 2010; Audard et al. 2014; Cody et al. 2014). Therefore, the study of disc longevity typically relies on disc population statistics rather than observations of individual systems.

The earliest empirical study of disc longevity was carried out by Strom et al. (1989), who found that the fraction of stars with hot inner accretion discs, detected by *K*-band excess and Hα emission (associated with classical T-Tauri stars), diminishes significantly for stars older than 3 Myr in the Taurus–Auriga star-forming region (SFR).

In the seminal study of Haisch, Lada & Lada (2001b), the authors plot the fraction of stars showing *L*-band excess, indicating a hot inner dust disc, as a function of age for several young-to-intermediate age clusters (2.5–30 Myr). They identify a clear trend wherein discs are depleted over the course of several million years. This basic methodology of comparing cluster disc fraction with average stellar age has been adopted by a number of groups for more clusters spanning a wider age range (Hernández et al. 2008; Mamajek 2009; Fedele et al. 2010; Bell et al. 2013; Cloutier et al. 2014; Ribas et al. 2014). In some cases, multiple disc indicators are used; Mamajek (2009), for instance, uses Hα emission, *L*-band excess, 3.6 μm excess, and infrared spectral energy distribution (SED) shape as indicators of the presence of a hot inner disc. There is some evidence that disc longevity depends on host star spectral type (e.g. Haisch, Lada & Lada 2001a; Hernández et al. 2005; Carpenter et al. 2006; Kennedy & Kenyon 2009; Hernández et al. 2010; Luhman & Mamajek 2012; Ribas, Bouy & Merín 2015), with higher mass stars appearing to shed their discs more quickly.

Fedele et al. (2010) consider the possibility that the dust and gas of a disc do not perfectly coevolve. They compare the fraction of young stellar objects (YSOs) showing spectroscopic evidence of accretion on to the star (Hα emission) with the fraction showing infrared excess (IRE) in *Spitzer*/IRAC bands (3.6–8.0 μm, revealing small grains in the inner several au of a disc). Exponential half-lives calculated based on spectroscopic signs of accretion are slightly shorter than those calculated based on IRE. This indicates that circumstellar gas and dust mostly coevolve, but that discs may retain a longer lived dusty component after the gas has been depleted.

One potentially significant limitation of some previous works is the differing sensitivity limits between disc-bearing and disc-free YSOs. Disc-bearing YSOs are usually detected through IRE, therefore point source catalogues compiled using infrared photometry are biased towards finding disc-bearing YSOs. An overestimation of disc fraction will translate into an overestimation of disc lifetimes. This effect may be particularly important among lower mass (i.e. intrinsically fainter) stars, potentially leading to an apparent mass dependence that is not physical.

Another major impediment to obtaining accurate disc dissipation time-scales is the absence of a reliable stellar chronometer. Ages of individual PMS stars as well as age spreads of PMS members in individual clusters and SFRs are not accurate due to an interplay of multiple factors, such as photometric variability from accretion and magnetic activity, different accretional histories, binarity, extinction uncertainty, veiling from accretion, scattering and absorption by discs, stellar interiors model uncertainties including inconsistent age predictions for intermediate-mass and lower mass stars, distance uncertainty, and others (e.g. Preibisch 2012; Getman et al. 2014; Jeffries 2017).

Recent empirical evidence points to persistent errors in standard theoretical PMS evolutionary models, both old generation, such as Baraffe et al. (1998), Siess, Dufour & Forestini (2000), and new generation, such as Baraffe et al. (2015), Dotter (2016), and Choi et al. (2016). This emerges independently from findings of inconsistent ages between intermediate-mass and low-mass stars (Pecaut & Mamajek 2016; Fang, Herczeg & Rizzuto 2017) derived from the Hertzsprung–Russell diagram (HRD) or photometric colour–magnitude diagram (CMD), failure of theoretical models to reproduce the observed parameters of stars in eclipsing binaries (Kraus et al. 2015), and disagreement between Li-based and HRD/CMD-based ages (Jeffries et al. 2017). Specifically, the HRD locations of observed eclipsing binaries suggest that theoretical models underpredict (by 5–20 per cent) the stellar radii and overpredict $T_{\rm eff}$ (by 5–10 per cent) of low-mass ($M < 1$ M$_\odot$) PMS and MS stars, a phenomenon referred to as 'radius inflation'. Empirical correlations of inflation with rotation and magnetic activity (Somers & Stassun 2017) suggest that magnetic fields drive radius inflation. Recent attempts to account for magnetic effects include two types of models: global magnetic fields threaded into the stellar interior (Feiden 2016) and starspot flux blocking (Somers & Pinsonneault 2015). Both models lead to changes in the stellar structure that reproduce true radius sizes.

Some of the previous works on cluster disc fraction including Haisch et al. (2001b), Hernández et al. (2008), Mamajek (2009), Fedele et al. (2010), and Ribas et al. (2014) employ literature compilations of heterogeneous sets of cluster members and/or heterogeneous estimates of cluster ages. Examples of obvious sources of heterogeneity, which lead to uncertainty and scatter in age estimates, include differing data wavelength ranges, types of data (e.g. photometry versus spectroscopy), age methods (e.g. HRD, CMD, disc fraction, kinematic, etc.), stellar mass ranges, ways of transformation between theory and observation, subcluster membership in SFRs and others (e.g. Soderblom et al. 2014). Application of differing PMS evolutionary models to the same set of data would generally lead to systematic shifts in age estimates. None of the aforementioned studies considered the impact of differing PMS models on their disc longevity estimates.

To investigate some of the aforementioned issues in detail, we employ the data from the Massive Young Star-Forming Complex Study in Infrared and X-ray (MYStIX, Feigelson et al. 2013) and Star Formation in Nearby Clouds (SFiNCs, Getman et al. 2017) projects. Both data sets incorporate *Chandra* X-ray data to help identify disc-free YSOs in 42 total young SFRs. In the current work, we use YSO classifications (disc-bearing versus disc-free) of X-ray and infrared point sources along with homogeneous sets of cluster ages (Getman et al. 2014) for 69 clusters spread across 32 of the total 42 MYStIX and SFiNCs target regions (Kuhn et al. 2014; Getman et al. 2018) to study effects of differing PMS evolutionary models, mass, star-forming environments, and initial disc fractions on disc longevity. Ten MYStIX/SFiNCs regions without cluster membership assignments and/or sufficient numbers of stars with available age estimates and disc classes were excluded from our disc fraction analyses (Section 2.1).

YSO candidate selection and cluster membership determination are described in Section 2.1. The classification of disc-bearing and disc-free YSOs is summarized in Section 2.2. Age estimation for MYStIX and SFiNCs clusters using multiple PMS evolutionary models is given in Section 2.3. Our strategy for mitigating the problem of differential mass sensitivities for disc-bearing and disc-free YSOs is discussed in Section 2.4. The main results for disc longevity are discussed in Section 3, including the impacts of different factors (classification of YSOs on disc-bearing and disc-free, assumption of initial disc fraction, choice of PMS model, effects of stellar star-forming environments and mass) on our disc longevity

estimates. Further discussion, comparison with previous literature, and suggestions for future work are presented in Section 4.

2 METHODS

2.1 Cluster membership

The MYStIX probable cluster member catalog contains cross-matched X-ray (*Chandra*/ACIS), near-infrared (2MASS or UKIDSS), and mid-infrared (*Spitzer*/IRAC; 3.6–8.0 μm) point sources. IRE selection captures PMS stars with hot inner discs while X-ray selection captures PMS stars with strong magnetic flaring activity. IRE stars are found by comparing the 1–8 μm SEDs to circumstellar disc models (Povich et al. 2013) while X-ray stars are found with a naive Bayes classifier that tales a variety of properties into account (Broos et al. 2013). Generally in MYStIX, the *Chandra* samples are larger than the IRE samples, but there is often considerable overlap in members identified by the two methods. Detailed discussion of catalogue assembly and membership selection is provided by Feigelson et al. (2013) and other MYStIX papers (Kuhn et al. 2013a,b; Naylor, Broos & Feigelson 2013; Povich et al. 2013; Townsley et al. 2014). The full list of ∼32 000 MYStIX probable YSO members is given by Broos et al. (2013); and Kuhn et al. (2014) identify 142 clusters across 17 MYStIX regions by fitting isothermal ellipsoids to the star locations.

The same MYStIX-based X-ray and IR data analysis methods are used for the reanalysis of the archived *Chandra* and *Spitzer* data for the nearby 22 SFiNCs SFRs (Getman et al. 2017). Due to the smaller cluster distances and higher Galactic latitudes of the SFiNCs SFRs compared to MYStIX ones, the IR counterpart and YSO membership identifications are achieved using simpler methods than in MYStIX, such as traditional proximity and decision tree membership classification methods (Getman et al. 2017). The full list of nearly 8500 SFiNCs probable YSO members is given by Getman et al. (2017). Getman et al. (2018) identify 52 clusters and 19 unclustered stellar structures across the 22 SFiNCs SFRs using the methods of Kuhn et al. (2014). For our disc longevity analysis, the 19 unclustered stellar structures are each treated as a single cluster. Throughout the remainder of this paper, the term 'cluster' will also apply to these 19 unclustered components.

Sensitivity and completeness levels of the MYStIX and SFiNCs YSO catalogues vary among the regions due to differing distances, observation exposures, and absorptions across the fields, as well as due to differing levels of diffuse IR nebular background. For instance, the very deep X-ray exposure of the nearby ONC cluster reaches the completeness limits of ∼0.1–0.2 $M_{\odot}$, while the deep X-ray exposure of the most distant MYStIX region NGC 1893 allows a nearly complete detection of PMS stars only above ∼1–2 $M_{\odot}$ (see fig. 1 in Kuhn, Getman & Feigelson 2015a). For more distant ($d > 1$ kpc) MYStIX regions, the 2MASS limiting sensitivity of $K_s \sim 14.3$ mag becomes inadequate for identifying YSO counterparts to *Chandra* sources; thus for most of these regions, the 2MASS catalogue is complemented by the deeper UKIRT catalog, when available (Feigelson et al. 2013). The *Chandra* X-ray-selected and *Spitzer* mid-infrared-selected MYStIX/SFiNCs YSO samples generally have different sensitivities within individual regions; for instance, an X-ray selected YSO portion is deeper for Be 59 (see fig. 12 in Getman et al. 2017), but a mid-infrared-selected portion is deeper for W 40 (see fig. 8 in Kuhn et al. 2015b).

Due to the omission of *Spitzer*-MIPS and far-infrared data, MYStIX and SFiNCs lack the ability to identify some fraction of protostellar objects and transition disc objects (systems with inner disc holes or optically thin inner discs), especially those that were not detected in X-rays. Since the ages of the MYStIX and SFiNCs clusters are estimated based on PMS samples (Section 2.3), we are instead interested in characterization of disc fractions for YSO samples, from which the remaining protostars are removed (Section 2.2).

The membership algorithms applied to the MYStIX and SFiNCs X-ray, NIR, and MIR catalogues produce small fractions of false positives. For instance, table 8 in Broos et al. (2013) shows an excellent (within a few to several per cent) agreement between the numbers of the simulated and identified and removed extragalactic and Galactic field contaminants. Getman et al. (2017) estimate that less than a few per cent of contaminants, mainly field stars, could be present within the SFiNCs sample of YSOs. Getman et al. further compare SFiNCs with previously published YSO catalogues. As an example of the low contamination in SFiNCs membership, here we consider IC 348, one of the richest nearby SFRs. Table 9 and figs 12, 17, and 18 in Getman et al. show that the SFiNCs YSO identification is in good agreement with the recent optical/infrared spectroscopic/photometric YSO catalogue of Luhman, Esplin & Loutrel (2016, hereafter Lu16). Out of the 478 Lu16 YSOs, 77 per cent are identified by SFiNCs. Half of the remaining 23 per cent (generally IR brighter) lie outside the SFiNCs X-ray fields, and the other half (IR weaker) are very low-mass stellar and brown dwarf candidates ($M \lesssim 0.1$ $M_{\odot}$) undetectable in the SFiNCs X-ray exposures. On the other hand, additional to Lu16, SFiNCs identifies 29 new YSOs; of those half are disc-free and half are disc-bearing; over two-thirds are X-ray detected. The fact that the vast majority of these are not distributed randomly across the SFiNCs X-ray field but are rather spatially concentrated in the southern part of the field, right outside the primary membership area of Lu16 ($r = 14$ arcmin; their fig. 1), and have IR/X-ray colours consistent with those of the other YSOs, gives confidence that these are real YSOs and not source contaminants.

Only a portion of the full MYStIX and SFiNCs samples can be used for our effort to understand disc evolution. Specifically, we require clusters with available Age_{JX} estimates (Section 2.3) and at least 10 disc-bearing and 10 disc-free YSOs within each cluster *prior* to the imposition of mass cuts described in Section 2.4. The resulting subsample consists of 7100 MYStIX YSOs in 34 clusters, and 5834 SFiNCs YSOs in 35 clusters. These numbers of YSOs are further reduced after the imposition of mass cuts (Section 2.4); and the numbers vary among the four different membership permutations considered in the current study (Section 2.2). The final YSO numbers are listed in Tables 1 and 2.

2.2 YSO classification

There is no consensus on criteria for discriminating between disc-bearing and disc-free stars. We apply and compare two schemes for doing so. In the first, we use the classifications found in the MYStIX and SFiNCs catalogues derived in the following ways. For MYStIX, Povich et al. (2013) classify YSOs by fitting JHK_s and *Spitzer*/IRAC photometry with the model SEDs of Robitaille et al. (2006, discs) and Castelli & Kurucz (2004, stellar photospheres), and removing numerous contaminating sources (extragalactic objects, asymptotic giant branch stars, nebular knots, and unrelated YSOs) through additional infrared colour cuts and spatial clustering analyses. X-ray detections, an indicator of youth, are required for disc-free YSOs in order to exclude field stars. SFiNCs regions are out of the Galactic plane and therefore suffer from less contamination than MYStIX regions. Getman et al. (2017) therefore classify SFiNCs YSOs using simpler procedures, namely, the *Spitzer*/IRAC

Table 1. Properties of 69 MYStIX and SFiNCs clusters. This version of the table lists 69 entries (one per cluster) corresponding to the membership case with $\alpha_{\rm IRAC}$-based classification and probable protostars included. This table is available in its entirety (69 × 4 entries) in the Supplementary Materials. That is, the on-line table version gives four entries per cluster, one for each of the four membership permutations yielded by using two different YSO classification schemes (YSO Classes = Catalogue and YSO Classes = $\alpha_{\rm IRAC}$) and including and excluding probable protostars. Here, Column 1: Cluster of interest. Column 2: Distances from the Sun, taken from Feigelson et al. (MYStIX; 2013) and Getman et al. (SFiNCs; 2017). Columns 3–5: Cluster ages using three different PMS evolutionary models. Columns 6–7: Minimum mass cut-off and median stellar mass in a cluster (based on the Siess00 age scale). Columns 8–9: Numbers of disc-bearing ($N_{\rm disc}$) and disc-free ($N_{\rm nodisc}$) YSOs after the imposition of $M_{\rm cut}$. Column 10: Inferred disc fraction $f_{\rm disc} = N_{\rm disc}/(N_{\rm disc} + N_{\rm nodisc})$.

Region/Cluster	D	Age_{JX} Siess00	Age_{JX} MIST	Age Feiden16M	$M_{\rm cut}$ Siess00	Median mass Siess00	$N_{\rm disc}$	$N_{\rm nodisc}$	$f_{\rm disc}$
	(kpc)	(Myr)	(Myr)	(Myr)	($M_\odot$)	($M_\odot$)			
(1)	(2)	(3)	(4)	(5)	(6)	(7)	(8)	(9)	(10)
				MYStIX					
Eagle/A	1.75	2.4 ± 1.0	2.0 ± 0.8	4.5	0.95	1.24	3	13	$0.19^{+0.12}_{-0.19}$
Eagle/B	1.75	2.1 ± 0.1	1.5 ± 0.1	3.6	0.25	1.17	295	348	$0.46^{+0.04}_{-0.04}$
Eagle/D	1.75	2.5 ± 0.2	1.6 ± 0.2	3.8	0.16	1.47	151	153	$0.50^{+0.06}_{-0.06}$
Flame/A	0.414	0.8 ± 0.2	0.4 ± 0.1	1.5	0.10:	0.38	101	41	$0.71^{+0.08}_{-0.07}$
Lagoon/A	1.3	2.2 ± 0.2	1.7 ± 0.1	4.0	0.18:	0.69	16	11	$0.59^{+0.19}_{-0.16}$
Lagoon/C	1.3	1.6 ± 0.2	1.0 ± 0.3	2.7	0.11:	1.13	19	12	$0.61^{+0.17}_{-0.15}$
Lagoon/E	1.3	1.9 ± 0.2	1.4 ± 0.2	3.4	0.11:	1.06	34	44	$0.44^{+0.10}_{-0.11}$
Lagoon/F	1.3	2.3 ± 0.1	1.8 ± 0.2	4.2	0.12	0.96	108	153	$0.41^{+0.06}_{-0.06}$
Lagoon/H	1.3	2.1 ± 0.4	1.3 ± 0.3	3.2	0.10:	1.25	47	43	$0.52^{+0.10}_{-0.10}$
Lagoon/I	1.3	2.1 ± 0.2	1.5 ± 0.2	3.6	0.10:	0.97	79	85	$0.48^{+0.08}_{-0.08}$
Lagoon/J	1.3	2.7 ± 0.2	1.9 ± 0.3	4.4	0.11:	1.28	19	32	$0.37^{+0.12}_{-0.14}$
Lagoon/K	1.3	1.4 ± 0.2	1.0 ± 0.2	2.6	0.11:	1.19	60	28	$0.68^{+0.10}_{-0.09}$
M 17/D	2.0	1.1 ± 0.2	0.7 ± 0.1	2.0	0.12:	3.68	21	14	$0.60^{+0.16}_{-0.14}$
NGC 1893/A	3.6	3.5 ± 1.0	2.7 ± 0.9	5.9	0.19:	1.81	21	39	$0.35^{+0.11}_{-0.13}$
NGC 1893/B	3.6	2.6 ± 0.3	2.0 ± 0.3	4.7	0.09:	1.15	56	68	$0.45^{+0.08}_{-0.09}$
NGC 1893/I	3.6	2.8 ± 0.6	1.9 ± 0.3	4.3	0.12:	1.36	66	51	$0.56^{+0.09}_{-0.09}$
NGC 2264/E	0.913	3.2 ± 0.5	2.4 ± 0.7	5.4	0.10:	0.58	17	58	$0.23^{+0.08}_{-0.11}$
NGC 2264/J	0.913	1.6 ± 0.7	1.2 ± 0.6	3.0	0.10:	0.75	35	15	$0.70^{+0.14}_{-0.11}$
NGC 2264/K	0.913	2.2 ± 0.3	1.5 ± 0.2	3.6	0.09:	0.66	39	31	$0.56^{+0.12}_{-0.11}$
NGC 2362/B	1.48	2.9 ± 0.2	2.1 ± 0.2	4.8	0.09:	0.50	23	177	$0.12^{+0.04}_{-0.05}$
NGC 6334/B	1.7	2.3 ± 0.4	1.8 ± 0.5	4.1	0.17:	1.92	26	14	$0.65^{+0.15}_{-0.13}$
NGC 6334/J	1.7	1.5 ± 0.4	0.9 ± 0.4	2.3	0.11:	3.85	20	4	$0.83^{+0.19}_{-0.10}$
NGC 6334/L	1.7	0.7 ± 0.3	0.4 ± 0.2	1.4	0.39	1.60	20	1	$0.95^{+0.18}_{-0.04}$
NGC 6357/A	1.7	1.4 ± 0.1	0.9 ± 0.1	2.4	0.13:	1.58	60	64	$0.48^{+0.09}_{-0.09}$
NGC 6357/B	1.7	1.4 ± 0.2	1.0 ± 0.2	2.6	0.09:	1.46	94	62	$0.60^{+0.08}_{-0.07}$
NGC 6357/C	1.7	1.2 ± 0.3	0.9 ± 0.2	2.4	0.41	1.38	71	67	$0.51^{+0.08}_{-0.08}$
NGC 6357/E	1.7	1.4 ± 0.4	0.9 ± 0.3	2.3	0.14:	1.86	38	26	$0.59^{+0.12}_{-0.11}$
NGC 6357/F	1.7	1.5 ± 0.2	1.0 ± 0.2	2.6	0.11:	1.79	90	72	$0.56^{+0.08}_{-0.07}$
RCW 36/A	0.7	0.9 ± 0.1	0.5 ± 0.1	1.6	0.09:	0.35	105	24	$0.81^{+0.08}_{-0.06}$
Rosette/E	1.33	3.0 ± 0.2	2.3 ± 0.1	5.3	0.21	0.66	130	335	$0.28^{+0.04}_{-0.04}$
Rosette/L	1.33	2.7 ± 0.7	1.9 ± 1.0	4.3	0.10:	0.81	136	95	$0.59^{+0.06}_{-0.06}$
Rosette/M	1.33	1.9 ± 0.4	1.4 ± 0.3	3.3	0.11:	0.81	43	8	$0.84^{+0.12}_{-0.08}$
Rosette/N	1.33	1.3 ± 1.4	0.7 ± 1.0	2.0	0.12:	0.68	14	15	$0.48^{+0.17}_{-0.17}$
W 40/A	0.5	0.8 ± 0.1	0.4 ± 0.1	1.5	0.10:	0.53	123	33	$0.79^{+0.07}_{-0.06}$
				SFiNCs					
Be 59/A	0.9	1.8 ± 0.2	1.4 ± 0.2	3.3	0.10:	0.78	149	152	$0.50^{+0.06}_{-0.06}$
Be 59/B	0.9	2.2 ± 0.4	1.6 ± 0.3	3.8	0.75	1.59	35	60	$0.37^{+0.09}_{-0.10}$
Cep A/A	0.7	1.4 ± 0.3	1.0 ± 0.2	2.6	0.10:	0.38	50	27	$0.65^{+0.11}_{-0.10}$
Cep A/U	0.7	2.0 ± 0.3	1.4 ± 0.3	3.3	0.10:	0.43	29	57	$0.34^{+0.09}_{-0.10}$
Cep C/U	0.7	2.2 ± 0.9	2.0 ± 0.6	4.6	0.10:	0.47	26	33	$0.44^{+0.12}_{-0.13}$
Cep OB3b/A	0.7	2.2 ± 0.2	1.9 ± 0.2	4.4	0.09:	0.36	201	195	$0.51^{+0.05}_{-0.05}$
Cep OB3b/C	0.7	2.4 ± 0.1	2.0 ± 0.1	4.6	0.09:	0.44	284	324	$0.47^{+0.04}_{-0.04}$

Table 1 – *continued*

Region/Cluster	D	Age_{JX} Siess00	Age_{JX} MIST	Age Feiden16M	M_{cut} Siess00	Median mass Siess00	N_{disc}	N_{nodisc}	f_{disc}
	(kpc)	(Myr)	(Myr)	(Myr)	($M_\odot$)	($M_\odot$)			
(1)	(2)	(3)	(4)	(5)	(6)	(7)	(8)	(9)	(10)
Cep OB3b/U	0.7	3.4 ± 0.4	2.5 ± 0.6	5.6	0.10:	0.42	33	48	$0.41^{+0.10}_{-0.11}$
GGD 12-15/A	0.83	0.6 ± 0.6	0.4 ± 0.6	1.4	0.10:	0.34	44	11	$0.80^{+0.12}_{-0.08}$
GGD 12-15/U	0.83	2.5 ± 0.5	2.2 ± 0.4	5.0	0.11:	0.43	31	57	$0.35^{+0.09}_{-0.10}$
IC 348/B	0.3	2.5 ± 0.1	2.0 ± 0.2	4.6	0.09:	0.36	91	129	$0.41^{+0.06}_{-0.07}$
IC 348/U	0.3	3.8 ± 0.4	3.4 ± 0.6	7.4	0.11:	0.35	11	27	$0.29^{+0.12}_{-0.16}$
IC 5146/B	0.8	1.5 ± 0.2	1.2 ± 0.2	3.1	0.10:	0.57	88	37	$0.70^{+0.09}_{-0.07}$
IC 5146/U	0.8	2.6 ± 0.5	2.0 ± 0.3	4.6	0.30	0.67	37	34	$0.52^{+0.11}_{-0.11}$
IRAS 00013+681/A	0.9	1.8 ± 1.8	1.2 ± 1.4	3.0	0.18	0.68	24	9	$0.73^{+0.17}_{-0.12}$
IRAS 20050+2720/U	0.7	3.3 ± 0.4	2.6 ± 0.4	5.8	0.57	0.99	8	20	$0.29^{+0.13}_{-0.18}$
LkHα 101/A	0.51	1.5 ± 0.3	1.0 ± 0.3	2.6	0.09:	0.37	78	62	$0.56^{+0.08}_{-0.08}$
LkHα 101/U	0.51	2.2 ± 0.6	1.7 ± 0.5	4.0	0.10:	0.34	23	22	$0.51^{+0.14}_{-0.14}$
Mon R2/A	0.83	1.2 ± 0.1	0.9 ± 0.1	2.4	0.09:	0.28	65	13	$0.83^{+0.10}_{-0.07}$
Mon R2/U	0.83	1.7 ± 0.2	1.4 ± 0.2	3.3	0.09	0.47	134	74	$0.64^{+0.07}_{-0.06}$
NGC 1333/A	0.235	2.5 ± 1.2	1.2 ± 1.5	3.0	0.09:	0.17	16	6	$0.73^{+0.21}_{-0.14}$
NGC 1333/B	0.235	1.7 ± 0.3	1.3 ± 0.3	3.2	0.09:	0.18	29	15	$0.66^{+0.15}_{-0.12}$
NGC 2068/B	0.414	1.2 ± 0.2	0.7 ± 0.1	2.0	0.10:	0.43	57	34	$0.63^{+0.10}_{-0.09}$
NGC 2068/D	0.414	1.0 ± 0.3	0.6 ± 0.2	1.8	0.11:	0.59	23	11	$0.68^{+0.17}_{-0.13}$
NGC 2068/U	0.414	2.3 ± 0.4	1.4 ± 0.5	3.4	0.09:	0.41	37	40	$0.48^{+0.11}_{-0.11}$
OMC 2-3/U	0.414	1.7 ± 0.2	1.2 ± 0.2	3.0	0.09:	0.32	81	100	$0.45^{+0.07}_{-0.07}$
ONC Flank N/A	0.414	1.7 ± 0.2	1.2 ± 0.2	3.0	0.13	0.52	80	104	$0.43^{+0.07}_{-0.07}$
ONC Flank S/A	0.414	1.6 ± 0.2	1.1 ± 0.1	2.8	0.09:	0.41	114	122	$0.48^{+0.06}_{-0.06}$
RCW 120/B	1.35	0.8 ± 0.2	0.6 ± 0.1	1.8	0.36:	1.41	41	32	$0.56^{+0.11}_{-0.11}$
RCW 120/C	1.35	0.7 ± 0.4	0.5 ± 0.3	1.6	0.19:	1.07	26	10	$0.72^{+0.16}_{-0.12}$
RCW 120/U	1.35	1.2 ± 0.2	0.9 ± 0.2	2.5	0.15:	0.91	22	40	$0.35^{+0.11}_{-0.12}$
Serpens Main/B	0.415	0.6 ± 0.7	0.3 ± 0.8	1.2	0.10:	0.64	14	10	$0.58^{+0.19}_{-0.17}$
Serpens Main/U	0.415	2.2 ± 0.5	1.5 ± 0.5	3.6	0.09:	0.19	17	19	$0.47^{+0.15}_{-0.16}$
Serpens South/U	0.415	1.8 ± 0.8	1.7 ± 0.6	4.0	0.11:	0.31	15	11	$0.58^{+0.19}_{-0.17}$
Sh 2-106/U	1.4	0.8 ± 0.4	0.6 ± 0.4	1.7	0.13:	0.60	49	43	$0.53^{+0.10}_{-0.10}$

Table 2. Disc longevity estimates ($f_0 = 100$ per cent).

Project	YSO classes	Incl. possible protostars?	N_{disc}	N_{nodisc}	$t_{1/2}$ (Myr)	SSR
(1)	(2)	(3)	(4)	(5)	(6)	(7)
MYStIX	Catalogue	N	1329	1606	$1.7^{+0.3}_{-0.2}$	0.90
MYStIX	Catalogue	Y	1523	1675	$1.9^{+0.3}_{-0.3}$	0.95
MYStIX	α_{IRAC}	N	1924	2229	$1.8^{+0.2}_{-0.2}$	0.53
MYStIX	α_{IRAC}	Y	2180	2236	$1.9^{+0.3}_{-0.2}$	0.61
SFiNCs	Catalogue	N	1971	1778	$2.1^{+0.3}_{-0.2}$	0.61
SFiNCs	Catalogue	Y	2088	1761	$2.2^{+0.3}_{-0.2}$	0.55
SFiNCs	α_{IRAC}	N	1924	1971	$1.9^{+0.2}_{-0.2}$	0.59
SFiNCs	α_{IRAC}	Y	2062	1988	$2.0^{+0.2}_{-0.2}$	0.54

colour–colour diagram scheme of Gutermuth et al. (2009) combined with the SED-based analysis of Getman et al. (2012). We refer to this first set of YSO classifications collectively as 'catalogue class'.

Our second YSO classification scheme is based on apparent (non-dereddened) *Spitzer*/IRAC SED slopes, $\alpha_{IRAC} = d\log(\lambda F_\lambda)/d\log(\lambda)$, measured in the IRAC wavelength range from 3.6 to 8.0 μm. Available magnitudes in the 3.6, 4.5, 5.8, and 8.0 μm bands were used for the calculation of 100 per cent, 100 per cent, 64 per cent, and 49 per cent of the SED slopes, respectively. We use a critical value of $\alpha_{IRAC} = -1.9$ to distinguish between disc-bearing and disc-free YSOs. In Fig. 1, we plot kernel density distributions of α_{IRAC} for MYStIX and SFiNCs,

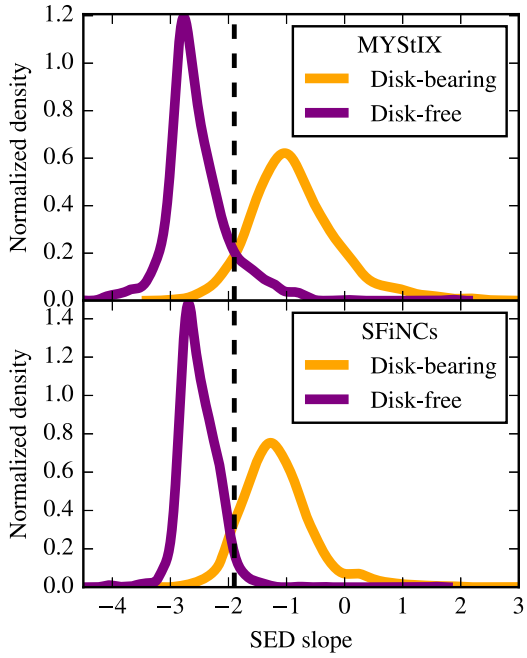

Figure 1. Kernel density estimation of SED slopes $\alpha_{\rm IRAC}$ for MYStIX (upper panel) and SFiNCs (lower panel) YSOs.

separately for disc-bearing and disc-free objects as determined by catalogue class (discussed in the previous paragraph). In both figures, the crossover point between disc-bearing and disc-free is close to −1.9. For MYStIX, 91 per cent of disc-bearing YSOs have $\alpha_{\rm IRAC} > -1.9$, while 86 per cent of disc-free YSOs have $\alpha_{\rm IRAC} < -1.9$. For SFiNCs, 91 per cent of disc-bearing YSOs have $\alpha_{\rm IRAC} > -1.9$, while 96 per cent of SFiNCs disc-free YSOs have $\alpha_{\rm IRAC} < -1.9$. The separation between disc-bearing and disc-free objects therefore appears to be consistent between MYStIX and SFiNCs. The two YSO classification schemes disagree for <14 per cent (<9 per cent) of the MYStIX (SFiNCs) stars.

For both YSO classification schemes, we repeat our analysis (presented in Section 3) while excluding probable protostars. We define probable protostars as being those objects with (non-dereddened) $\alpha_{\rm IRAC} > 0$.

We utilize both of the aforementioned schemes not only to compare these approaches – model SED-fitting, colour–colour diagrams, and infrared slope-based classifications are all widely used in the literature – but also due to the fact that model SED fitting and colour–colour based schemes yield many ambiguous classifications, including due to transition discs. The latter typically show weak or no IR excesses in the IRAC bands, adding to the uncertainties in disc classification and resulting disc fraction.

2.3 Cluster ages

MYStIX and SFiNCs cluster ages are determined using the Age_{JX} method described by Getman et al. (2014). Age_{JX} is applicable only to low-mass PMS stars [$M < 1.2$ M$_\odot$ assuming the Siess et al. (2000) age scale] with reliable measurements of the intrinsic X-ray luminosity and near-infrared $JHK_{\rm s}$ photometry. X-ray luminosities ($L_{\rm X}$) specify stellar mass according to the empirical PMS correlation seen in the Taurus region (Telleschi et al. 2007). J-band luminosities and mass estimates track with PMS evolutionary models, providing stellar ages. This yields homogeneous median age estimates for all 69 clusters used in the current analysis. To investigate how the choice of theoretical PMS evolutionary models affects disc dissipation time-scales, the Age_{JX} method is applied to the MYStIX and SFiNCs YSOs using a number of different models.

We start with four different sets of stellar evolutionary models: Siess et al. (2000, hereafter Siess00), Baraffe et al. (2015, hereafter Baraffe15), Dotter (2016) and Choi et al. (2016, hereafter MIST), and Feiden, Jones & Chaboyer (2015) and Feiden (2016, hereafter Feiden16). A quick examination of these models' evolutionary isochrones placed on the $L_{\rm bol}-T_{\rm eff}$ diagram suggests that, within the locus of the MYStIX/SFiNCs YSOs, the predictions of the Baraffe15 and MIST models are in good agreement with each other (figure not shown). Due to a poorer sampled published model grid, compared to MIST, the Baraffe15 model is omitted from further consideration. Compared to Siess00, newer generations of standard evolutionary models, such as Baraffe15 and MIST, with improved microphysics (including updated solar abundance scale, linelists, atmospheric convection parameters) predict systematically younger ages.

The Age_{JX} estimates for MYStIX and SFiNCs clusters based on the Siess00 model are already reported in Getman et al. (2014, 2018). Here we refer to these ages as Age_{JX}-Siess00. Next, we recalculate cluster ages using MIST as an underlying evolutionary model and following the same Age_{JX} procedure detailed in Getman et al. (2014). Here we refer to these ages as Age_{JX}-MIST. Briefly, the $L_{\rm X}$–mass relationship of Telleschi et al. (2007) is recalibrated by comparing the ($T_{\rm eff}$, $L_{\rm bol}$) measurements for Taurus X-ray emitting PMS stars (Güdel et al. 2007) to the MIST models. The X-ray luminosities of all Age_{JX} stars in MYStIX and SFiNCs are then converted to stellar masses. The differences between the resulting MIST and Siess00 based stellar masses are no more than 15 per cent. Comparison of absolute J-band magnitudes and masses with the MIST evolutionary tracks yields ages for individual stars. Cluster ages are then calculated as median ages of all Age_{JX} stellar cluster members. Statistical errors on cluster ages are calculated as 68 per cent confidence intervals using non-parametric bootstrap resampling. The bootstrap case resampling takes into account any forms of observed scatter; thus all sources of the scatter including the uncertainties on individual source extinctions, stellar masses, and local distances within the cluster (described in sections 3.3 and 5 in Getman et al. 2014) are treated naturally. Bootstrap does not treat 'systematic' uncertainties, such as the uncertainty in the knowledge of PMS evolutionary models or uncertainty on the distance from the Sun to the region (the latter is discussed in section 5 in Getman et al. 2014); such effects globally shift age scales.

The Dartmouth stellar evolution model grid (Dotter et al. 2008) extended to the PMS phase is used as a basis for the Feiden16 models (Feiden et al. 2015). Two versions of the Feiden16 models are provided, 'non-magnetic' and 'magnetic' (Feiden 2016). The published model grid is rather poorly sampled ($\Delta t = 0.5$ Myr) with no predictions for photometric magnitudes. Thus, the usage of the Age_{JX} method is not feasible here; and instead we opt for a simple age rescaling technique. In this approach, 5000 young stars within the parameter ranges of the MYStIX/SFiNCs-Age_{JX} stars are simulated on the $L_{\rm bol}$ versus $T_{\rm eff}$ diagram. Their ages are then derived using both the MIST and Feiden16 models. The resulting Feiden16 versus MIST age relationships are approximated by linear functions using standard major axis regression: $t_{F16,\rm non\text{-}magnetic} = 0.35 + 0.94 \times t_{\rm MIST}$ and $t_{F16,\rm magnetic} = 0.59 + 2.00 \times t_{\rm MIST}$.

Fig. 2 exemplifies comparison of the standard MIST and 'magnetic' Feiden16 models. Compared to MIST, the Feiden16 'magnetic' models predict systematically higher (by a factor of 1.6)

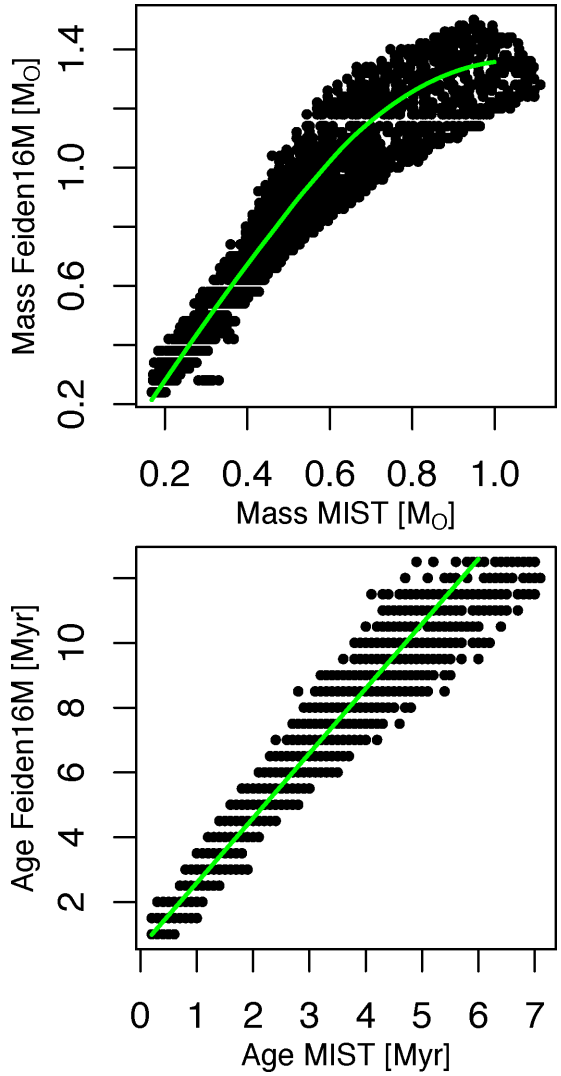

Figure 2. Comparison of the non-magnetic MIST (Choi et al. 2016; Dotter 2016) and magnetic Feiden16 (Feiden et al. 2015; Feiden 2016) PMS evolutionary models. Stellar masses (upper panel) and stellar ages (lower panel) resulted from the model fitting of simulated stars on the ($L_{\rm bol}$, $T_{\rm eff}$) diagram. The green curves are polynomial and linear (standard major axis) regression fits for the mass and age data, respectively. The polynomial and linear fits were obtained using the *R* (R Core Team 2014) functions *loess* and *lmodel2*, respectively.

masses and older (by a factor of 2−3) ages. Following the above equations, the *Age*$_{JX}$-MIST ages for the MYStIX/SFiNCs clusters are then transformed to *Age*-Feiden16 cluster ages. The 'non-magnetic' Feiden16 cluster ages are omitted from further consideration because they only slightly differ from the MIST ages (<30 per cent for 1 Myr and <10 per cent for >2 Myr clusters) and are systematically lower than the Siess00 ages. In contrast, the 'magnetic' Feiden16 cluster ages appear significantly higher than the MIST and Siess00 ages; we refer to these hereafter as *Age*-Feiden16M.

For all MYStIX/SFiNCs clusters, three types of cluster ages are reported in Table 1: old generation standard Siess00 (*Age*$_{JX}$-Siess00), new generation standard MIST (*Age*$_{JX}$-MIST), and new generation magnetic Feiden16 (*Age*-Feiden16M).

2.4 Stellar mass sensitivity

Given that discs around YSOs are detected using IRE, for a given infrared limiting magnitude, disc-bearing YSOs will be more readily detected than disc-free ones. Ignoring this sensitivity difference could lead to an erroneously high estimate of disc fraction – and therefore disc longevity – that reflects the underdetection of low-mass, disc-free YSOs. Note that this effect will manifest even if disc longevity does not vary with host star mass, and could wrongly lead to an *apparent* dependence of disc fraction on stellar mass.

In order to ensure that disc fractions are calculated within a similar range of stellar mass for each cluster, we choose a sensitivity limit for each cluster in the following way. Approximate stellar mass estimates are obtained based on star locations in the J versus $J-H$ CMD and theoretical stellar model tracks derived by Siess et al. (2000, for $M_\star < 7$ M$_\odot$) and Bressan et al. (2012, for $M_\star > 7$ M$_\odot$ stars). The reddening law of Rieke & Lebofsky (1985) is used to deredden the star positions to the intrinsic PMS model colours, assuming a single age (*Age*$_{JX}$-Siess00) for all the stellar members of a cluster. These mass estimates are subject to significant uncertainties and may be incompatible with individual masses obtained by other methods such as optical spectroscopy (Kuhn et al. 2010). However, the analysis of disc longevity as a function of stellar mass presented in Section 3.3.2 makes use of large stellar mass bins, so precise estimates of mass for individual objects are not required.

Once stellar masses have been calculated, we compare the stellar mass distributions of disc-bearing and disc-free YSOs in each of our 69 clusters. For each cluster, we iteratively remove the lowest mass YSO in the combined disc-bearing and disc-free sample until the Kolmogorov–Smirnov two-sample p-value exceeds 0.1. This yields a minimum mass cut-off $M_{\rm cut}$ for each cluster in order to ensure similar mass distributions and mass sensitivities for disc-bearing and disc-free YSOs. As mentioned in the next subsection, for many clusters, no YSOs are removed because they already show similar mass completeness for their disc-bearing and disc-free YSOs. Fig. 3 shows empirical cumulative distribution functions (ECDFs) of stellar mass for disc-bearing and disc-free objects in Rosette Nebula cluster E (NGC 2244; Kuhn et al. 2014), illustrating the derivation of $M_{\rm cut}$ and the effect of imposing it. For MYStIX clusters, typical values of $M_{\rm cut}$ typically range from 0.1 to 0.2 M$_\odot$, while for SFiNCs clusters, minimum stellar masses in the sample reach $\sim 0.1 M_\odot$, but no $M_{\rm cut}$ was applied due to the similar mass distributions of disc-bearing and disc-free stars.

Resulting subsamples of disc-bearing and disc-free stars, with similarly shaped mass ECDFs, are not affected by the choice of PMS evolutionary models insofar as both disc-bearing and disc-free samples are subject to the same mass transformation when transitioning among different PMS models. The mass scale itself changes; it is roughly similar between the Siess00 and MIST models, but shifts to higher values upon switching to the Feiden16M model (Section 2.3).

2.5 Summary of cluster data

Table 1 presents the cluster data.

Table 1 shows the following information for each of the 69 clusters studied in the current work: region name and cluster designation; three types of median ages (*Age*$_{JX}$-Siess00, *Age*$_{JX}$-MIST, and *Age*-Feiden16M); mass cut ($M_{\rm cut}$) and median stellar mass based on the Siess00 model; the number of disc-bearing ($N_{\rm disc}$) and disc-free ($N_{\rm nodisc}$) YSOs after the imposition of $M_{\rm cut}$; and disc fraction ($N_{\rm disc}/(N_{\rm disc} + N_{\rm nodisc})$). In the more complete, on-line version of

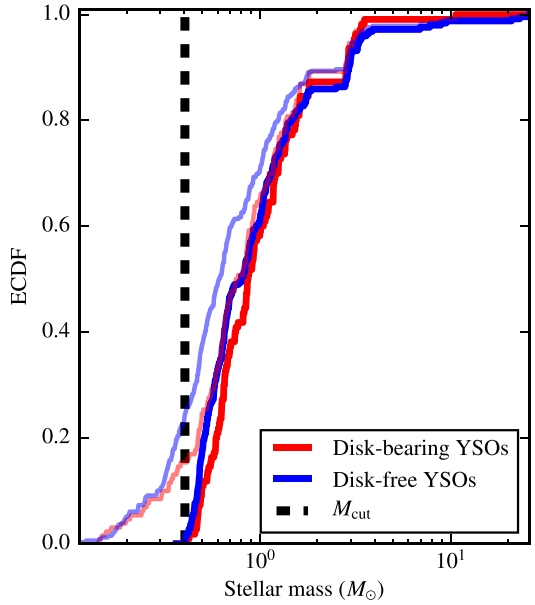

Figure 3. Comparison of stellar mass cumulative distributions for disc-bearing and disc-free YSOs in Rosette cluster E (NGC 2244), based on catalogue YSO classifications. The thinner (translucent) and thicker (solid) lines indicate the mass distributions before and after the imposition of M_{cut}, respectively.

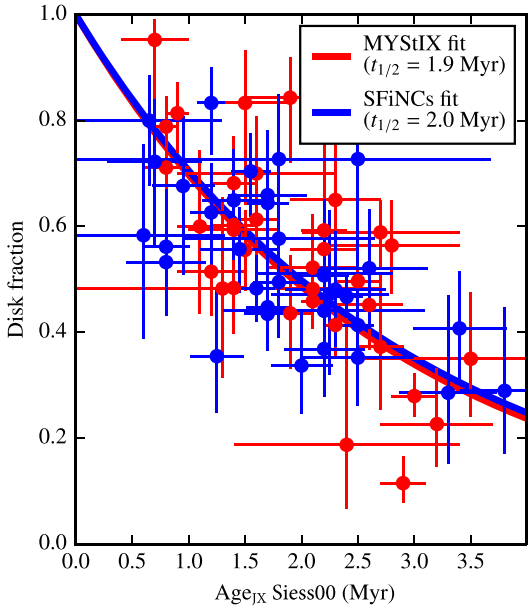

Figure 4. Disc fraction versus Age_{JX}-Siess00 for 69 MYStIX and SFiNCs clusters (red and blue points, respectively). The current figure exhibits results for one of the four membership permutations, that is, the α_{IRAC}-based YSO classification with probable protostars included. Figure panels showing disc fraction as a function of age for the other three permutations (based on catalogue YSO classification with/without probable protostars included and based on the SED slope YSO classification when probable protostars are excluded) are provided in the Supplementary Materials. Vertical error bars show Wilson binomial confidence intervals for confidence level 0.05.

Table 1, each cluster has four entries, one for each of the four permutations yielded by using two different YSO classification schemes (catalog classes versus α_{IRAC}-based) and including and excluding probable protostars.

A cluster designation of 'U' for an SFiNCs cluster indicates the unclustered component of a region. An M_{cut} value suffixed by a ':' indicates that no YSOs were removed from the sample according to the process described in the previous subsection, in which case the given value of M_{cut} indicates the lowest stellar mass in the sample for that cluster. Disc fraction uncertainties are Wilson confidence intervals for confidence level 0.05 (Wilson 1927; Brown, Cai & DasGupta 2001). Other properties of these SFiNCs and MYStIX clusters can be found in Getman et al. (2018) and Kuhn et al. (2014, 2015a,b).

3 RESULTS

In most of this section, we explore the effects of initial disc fraction (Sections 3.1.1 and 3.1.2), star-forming environment (Section 3.1.3), and stellar mass (Sections 3.3.1 and 3.3.2) on disc longevity, employing age, and mass results inferred from a single PMS evolutionary model, namely the Siess00 model. The effect of different PMS evolutionary models on disc longevity estimates is examined in Section 3.2 using the Siess00, MIST, and Feiden16M models.

3.1 Disc fraction versus age

3.1.1 With assumption of 100 per cent initial disc fraction

Here we produce a disc evolution plot resembling that of Haisch et al. (2001b) and other researchers. Cluster disc fraction as a function of Age_{JX}-Siess00 for 69 MYStIX and SFiNCs clusters is shown in Fig. 4. The four figure versions (available in the Supplementary Materials) reflect the four permutations of our analysis methods: two YSO classification schemes and two rules regarding the inclusion of probable protostars (Section 2.2). We perform a Gauss–Newton least-squares fit of an exponential function $f_{disc} = f_0 \times e^{-t/\tau}$ (with the mean lifetime τ as a free parameter) to each of the eight data sets (MYStIX and SFiNCs separately for each of the four membership permutations), assuming initial disc fraction $f_0 = 100$ per cent. The results are summarized in Table 2, along with the total number of disc-bearing and disc-free YSOs included in each analysis, as well as the sum of the squared residuals (SSR) for each exponential fit. The estimated disc half-life $t_{1/2} = \tau \times \ln(2)$ depends somewhat on the YSO classification scheme used, as well as on whether probable protostars are included in the sample, however the variation among these age estimates does not vary beyond their 95 per cent confidence intervals (shown in Table 2). The goodness of fit is better for SFiNCs regions, and is typically slightly better for the analyses using α_{IRAC}-based YSO classifications compared with those using catalogue classifications.

3.1.2 Without assumption of 100 per cent initial disc fraction

We explore the possibility that the zero-age disc fraction f_0 is less than 100 per cent. That is, some stars would be born without dusty circumstellar discs, or lose these discs very rapidly (<0.5 Myr). As in the previous subsection, we fit exponential functions, this time with f_0 as an additional parameter, using the adaptive non-linear least-squares algorithm of Dennis, Gay & Walsh (1981). Results are shown in Table 3. For MYStIX clusters, the exponential half-lives do not differ significantly from those reported in Table 2, though the uncertainties become considerably larger; the initial disc fractions remain consistent with 100 per cent. For SFiNCs clusters, the estimated half-lives are longer than those shown in Table 2,

Table 3. Disc longevity and initial disc fraction estimates ($f_0 < 100$ per cent).

Project	YSO classes	Incl. possible protostars?	$t_{1/2}$ (Myr)	f_0	SSR
(1)	(2)	(3)	(4)	(5)	(6)
MYStIX	Catalogue	N	$2.2^{+2.0}_{-0.7}$	$0.84^{+0.16}_{-0.21}$	0.79
MYStIX	Catalogue	Y	$2.3^{+2.2}_{-0.7}$	$0.87^{+0.13}_{-0.22}$	0.88
MYStIX	$\alpha_{\rm IRAC}$	N	$1.8^{+0.6}_{-0.2}$	$1.00^{+0.00}_{-0.18}$	0.53
MYStIX	$\alpha_{\rm IRAC}$	Y	$1.9^{+0.5}_{-0.2}$	$1.00^{+0.00}_{-0.13}$	0.61
SFiNCs	Catalogue	N	$3.5^{+3.9}_{-1.2}$	$0.77^{+0.16}_{-0.14}$	0.43
SFiNCs	Catalogue	Y	$3.2^{+2.7}_{-1.0}$	$0.83^{+0.16}_{-0.14}$	0.43
SFiNCs	$\alpha_{\rm IRAC}$	N	$3.2^{+2.9}_{-1.0}$	$0.75^{+0.16}_{-0.14}$	0.43
SFiNCs	$\alpha_{\rm IRAC}$	Y	$2.9^{+2.2}_{-0.9}$	$0.81^{+0.17}_{-0.15}$	0.44

but no more than 2σ. In the two SFiNCs analyses where probable protostars are excluded, the upper 95 per cent confidence intervals for f_0 only reach the low-90 per cent range, which leaves room for the possibility that not all YSOs begin with a hot inner dust disc.

The large uncertainties on the disc half-life estimates shown in Table 3 stem from not having clusters in our sample that are both younger than 0.5 Myr and significantly older than the estimated e-folding times. Future works that examine disc longevity over a larger age range and have much richer homogeneous cluster samples should omit the assumption of 100 per cent disc fraction at zero age, as well as explore other parametrizations of disc longevity, given that there is no physical basis for assuming an exponential decay.

3.1.3 Dependence on star-forming environment

Using the MYStIX and SFiNCs data sets, we attempt to test whether discs in the richer star-forming environments targeted by the MYStIX survey evolve differently from discs in the more sparse environments seen in SFiNCs fields. In particular, MYStIX clusters are often dominated by multiple O stars while SFiNCs clusters are generally dominated by a single massive star, typically a late-O or early-B.

Previous observations and theory suggest no strong effects by OB photoevaporation and/or dynamical interactions of cluster members on the inner parts of circumstellar discs. For instance, the results of Richert et al. (2015) suggest that external photoevaporation by OB stars does not affect the presence of IRE (nor is it likely to be based on theory, which does not predict significant truncation closer than ∼100 au to a disc's host star; e.g. Anderson, Adams & Calvet 2013). Meanwhile, theory regarding disc truncation due to dynamical encounters among YSOs does not predict disc depletion much closer to the star than ∼100 au, and certainly not within the few-au orbital radii associated with near-/mid-IRE (Portegies Zwart 2016; Vincke & Pfalzner 2016).

We find that the estimated values of $t_{1/2}$ and f_0 shown in Tables 2 and 3 do not differ beyond the expected statistical error between MYStIX and SFiNCs. Thus our data provide no evidence for distinctive dissipation time-scales of discs in different star-forming environments.

3.2 Effect of PMS evolutionary models on disc longevity

Here we investigate the effect of uncertainty in our knowledge of PMS evolution on disc longevity. We study disc fraction as a function of age using three different sets of cluster ages: the traditional *Age*$_{JX}$-Siess00, the new *Age*$_{JX}$-MIST with improved microphysics, and the new *Age*-Feiden16M that include 'radius inflation' due to magnetic fields (Section 2.3). This analysis is applied to the combined MYStIX+SFiNCs sample of 69 clusters using four different membership permutations (Table 4). Using the non-linear weighted Gauss–Newton least-squares method, the data sets are fitted with an exponential function $f_{\rm disc} = f_0 \times {\rm e}^{-t/\tau}$ with the mean lifetime τ as a free parameter and the initial disc fraction (f_0) fixed at 100 per cent.

Fig. 5 and Table 4 show that even though the goodness of fit is better for the cases with 'possible protostars included', the variations in $t_{1/2}$ due to different membership permutations are small (<15 per cent of a value) and are comparable to the statistical errors.

In contrast, the choice of different PMS models has a much stronger effect (70–170 per cent) on estimated $t_{1/2}$. The magnetic PMS models of Feiden (2016) lead to significantly longer disc dissipation time-scales ($t_{1/2,\rm Feiden16M} \sim 3.5$ Myr) compared to those of the non-magnetic models ($t_{1/2,\rm MIST,Siess00} \sim 1.3$–$2.0$ Myr). Clearly the choice of stellar evolutionary models, especially when magnetic fields are included, have a major effect on the inferred half-life of inner discs.

3.3 The role of stellar mass

Several previous works have indicated that discs survive longer around lower mass stars than around higher mass stars (Haisch et al. 2001a; Carpenter et al. 2006; Luhman & Mamajek 2012; Ribas et al. 2015).

In Section 3.3.1, we compare the properties of MYStIX and SFiNCs regions in order to determine differences in disc fraction due to the greater prevalence of higher mass stars in MYStIX than SFiNCs samples. In Section 3.3.2, we analyse the combined MYStIX and SFiNCs samples by binning YSOs according to age (*Age*$_{JX}$-Siess00) and stellar mass rather than by cluster.

3.3.1 Comparing MYStIX and SFiNCs clusters

We perform several comparisons of MYStIX and SFiNCs cluster properties. First, in Fig. 6, we compare ECDFs of median cluster ages (based on the Siess00 model) for MYStIX and SFiNCs. The ages of the MYStIX and SFiNCs cluster samples are similar.

Fig. 7 shows cluster disc fraction (across entire mass range and mass-stratified), median stellar mass (based on the Siess00 model), and median stellar mass by YSO type for the following analysis schemes, in order: catalogue YSO classifications and excluding probable protostars; catalogue YSO classifications and including probable protostars; $\alpha_{\rm IRAC}$-based YSO classifications and

Table 4. Disc longevity from the use of different PMS evolutionary models.

Project	PMS evolutionary model	YSO classes	Incl. possible protostars?	$t_{1/2}$ (Myr)	SSR
(1)	(2)	(3)	(4)	(5)	(6)
MYStIX+SFiNCs	Siess00	Catalogue	N	1.9 ± 0.2	2.23
MYStIX+SFiNCs	Siess00	Catalogue	Y	2.0 ± 0.2	1.52
MYStIX+SFiNCs	Siess00	$\alpha_{\rm IRAC}$	N	1.8 ± 0.1	1.64
MYStIX+SFiNCs	Siess00	$\alpha_{\rm IRAC}$	Y	1.9 ± 0.2	1.15
MYStIX+SFiNCs	MIST	Catalogue	N	1.4 ± 0.1	2.44
MYStIX+SFiNCs	MIST	Catalogue	Y	1.5 ± 0.2	1.66
MYStIX+SFiNCs	MIST	$\alpha_{\rm IRAC}$	N	1.3 ± 0.1	1.67
MYStIX+SFiNCs	MIST	$\alpha_{\rm IRAC}$	Y	1.4 ± 0.1	1.17
MYStIX+SFiNCs	Feiden16M	Catalogue	N	3.4 ± 0.3	2.06
MYStIX+SFiNCs	Feiden16M	Catalogue	Y	3.6 ± 0.4	1.43
MYStIX+SFiNCs	Feiden16M	$\alpha_{\rm IRAC}$	N	3.2 ± 0.2	1.46
MYStIX+SFiNCs	Feiden16M	$\alpha_{\rm IRAC}$	Y	3.5 ± 0.3	1.04

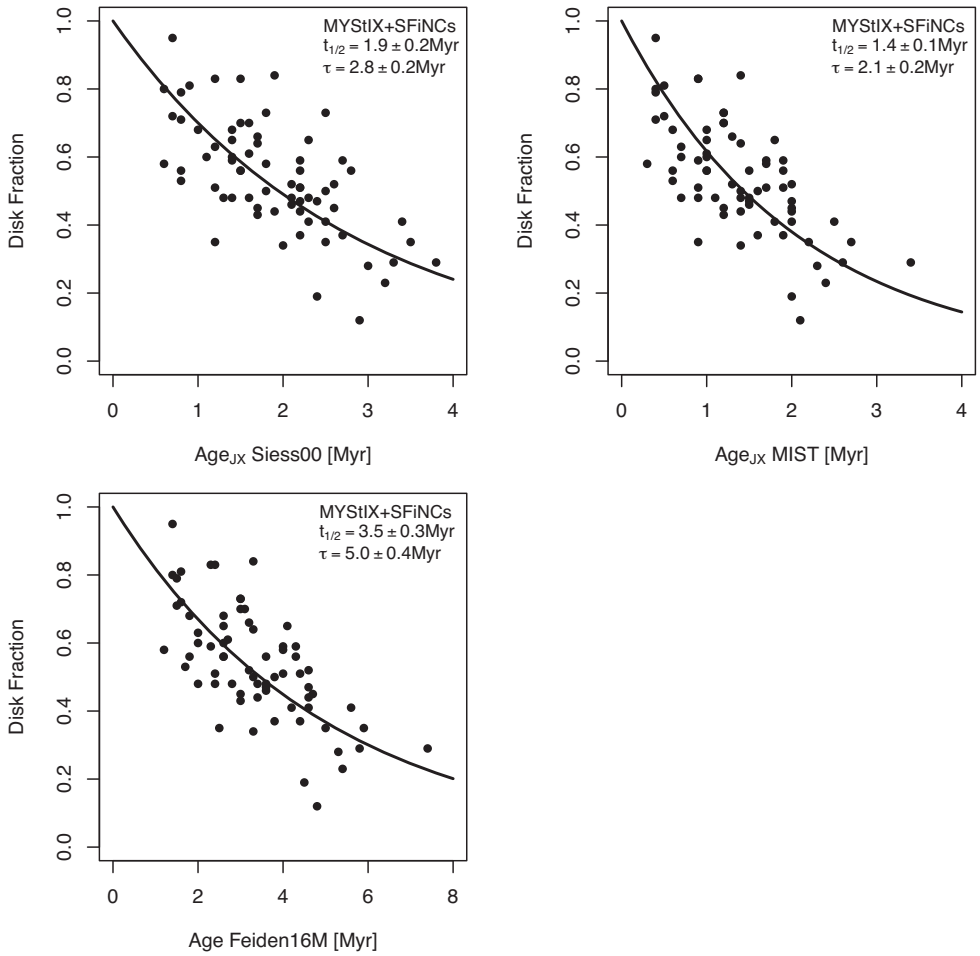

Figure 5. Disc fraction as a function of age using three types of cluster ages (Age_{JX}-Siess00, Age_{JX}-MIST, and *Age*-Feiden16M). The underlying data set (black points) is the combined MYStIX+SFiNCs sample of 69 clusters. The current figure exhibits results for one of the four membership permutations, that is, the $\alpha_{\rm IRAC}$-based YSO classification with probable protostars included. Figure panels showing disc fraction as a function of age for the other three permutations are provided in the Supplementary Materials. The black lines represent the best model fits. The figure legends provide disc dissipation time-scales resulting from the fits to an exponential model.

excluding probable protostars; and $\alpha_{\rm IRAC}$-based YSO classifications and including probable protostars.

The upper left panels of Fig. 7 show only modest differences in the distributions of disc fractions between MYStIX and SFiNCs clusters, which appear to stem largely from the presence of a handful of MYStIX clusters with low disc fractions. This is consistent with the similarity of the estimates of exponential disc half-life shown in Table 2, and does not provide strong evidence for

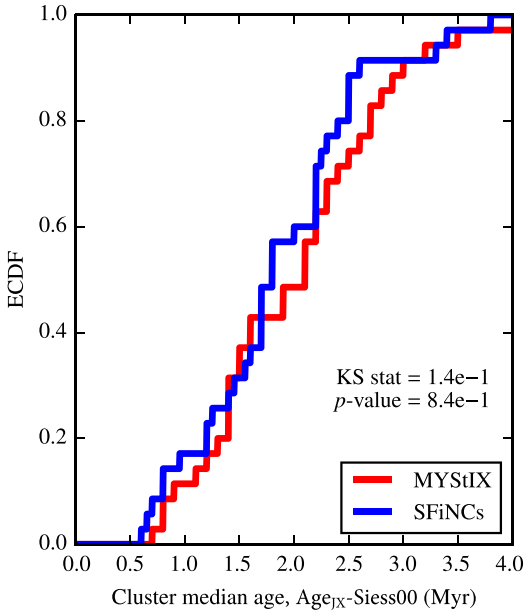

Figure 6. ECDF of median cluster ages (Age_{JX}-Siess00) for MYStIX (red) and SFiNCs (blue).

differential disc longevity between sparse (SFiNCs) and rich (MYStIX) SFRs.

The upper right panels of Fig. 7 show ECDFs of median cluster stellar mass for MYStIX and SFiNCs (YSO mass derivations are discussed in Section 2.5). MYStIX clusters have higher median masses for two reasons. First, MYStIX clusters are more distant, therefore a given magnitude limit in a given near-infrared band will translate into a higher stellar mass. Secondly, MYStIX clusters are richer and therefore physically contain more of the rare high-mass stars.

The lower left panels of Fig. 7 show ECDFs of subcluster median stellar mass separately for disc-bearing and disc-free YSOs, and separately for MYStIX and SFiNCs (median masses are calculated after $M_{\rm cut}$ has been applied). The disc-bearing and disc-free distributions are quite close to each other within both MYStIX and SFiNCs while the distributions between the two projects are quite different.

The lower right panels of Fig. 7 show ECDFs of disc fraction stratified by mass, separately for SFiNCs and MYStIX clusters. To mitigate the small number statistics issue (some clusters have only a few stars with $M > 2\,{\rm M}_{\odot}$) the mass cut-off is chosen here as $1\,{\rm M}_{\odot}$. The figure shows no differences in the distributions of disc fractions between higher and lower mass stars when using the $\alpha_{\rm IRAC}$-based YSO classifications. Only modest differences in the distributions of disc fractions for SFiNCs stars are present when using the catalogue YSO classifications; with a hint of possible age dependence – the SFiNCs clusters with higher disc fractions for more massive stars are, on average, slightly younger than the SFiNCs clusters with lower disc fractions for more massive stars. But this age difference is not statistically significant.

To summarize, for the same age range, MYStIX clusters have higher median masses (upper right and lower left panels of Fig. 7) than SFiNCs clusters. Any mass dependence of disc longevity thus should be apparent in the upper left and lower right panels of Fig. 7. The similarities of disc fractions between SFiNCs and MYStIX clusters when using the $\alpha_{\rm IRAC}$-based YSO classifications and only modest differences for some cluster subsamples when using the catalogue YSO classifications show that disc fraction is not strongly dependent on stellar mass. We explore this result in more detail in the following subsection.

3.3.2 *Disc longevity as a function of host star mass*

For the stellar population in the relatively old Upper Sco association ($t \sim 11$ Myr; Pecaut, Mamajek & Bubar 2012), Carpenter et al. (2006) and Luhman & Mamajek (2012) find that the more massive stars ($M > 1.2\,{\rm M}_{\odot}$) have a lower fraction of inner primordial discs. For the younger SFRs, NGC 1333 and IC 348 ($t \lesssim 3$ Myr), Luhman et al. (2016) find no signs of disc fraction variations within the spectral type range from L-type to B-type. Similarly, Kennedy & Kenyon (2009) find no significant differences in disc fraction between the $M < 1.5\,{\rm M}_{\odot}$ and $M > 1.5\,{\rm M}_{\odot}$ members of the younger, $t \lesssim 3$ Myr, stellar populations in Taurus, Cha I, and IC 348, but they provide observational evidence of stellar mass-dependent disc dispersal for older ($t > 3$ Myr) populations. In contrast, Ribas et al. (2015) suggest that the differences in the primordial disc fraction between the higher mass ($>2\,{\rm M}_{\odot}$) and lower mass ($<2\,{\rm M}_{\odot}$) stars are present even in younger ($t \lesssim 3$ Myr) regions, such as in the combined sample of Cha I, Cha II, CrA, Lupus, NGC 1333, σ Ori, Serpens, and Taurus.

Physically, this implies either an increased disc depletion rate due to accretion, photoevaporation, and planet(esimal) formation for higher mass host stars, or that initial disc fraction decreases with increasing stellar mass. In order to explore this question using the MYStIX and SFiNCs data sets, we place the YSOs that informed Fig. 4 into four stellar mass bins and four age bins; in other words, YSOs are now associated by age and mass, not by cluster. In this analysis, cluster ages and masses are derived based on the Siess00 model.

Disc fraction versus age for each of the four mass bins is shown in Fig. 8; the sample size within each mass bin is shown in the legend for each panel; with star numbers varying within the 1300–2800 range. The figure shows no statistically significant trends in disc fraction with stellar mass for young (<4 Myr; assuming the Siess00 age scale) clusters.

Surveys exclusively using infrared data to detect and classify YSOs may be at risk of underestimating the number of disc-free YSOs and thereby overestimating disc fraction (and subsequently disc longevity) among low-mass stars. By applying $M_{\rm cut}$ (Section 2.4), we ensure similar sensitivity to disc-bearing and disc-free YSOs.

However, our survey may have a bias against disc-free intermediate-mass stars because it relies on X-ray selection. It is well known that the X-ray sensitivity diminishes towards mid-B and mid-A type stars (e.g. Güdel & Nazé 2009; Stelzer et al. 2009; Drake et al. 2014). Such an X-ray sensitivity bias towards A- and B-type stars might lead to overestimation of disc fractions for our $>2\,{\rm M}_{\odot}$ stellar sample in Fig. 8, and thus prevent us from detecting the effect of lower disc fractions in higher mass stars reported in a number of previous disc fraction studies.

On the other hand, we consider our non-detection of such a trend to be consistent with the recent findings of Luhman et al. (2016) for the young ($t \lesssim 3$ Myr on the Siess00 age scale) IC 348 and NGC 1333 SFRs, which show no statistically significant variations in disc fraction for objects with spectral types between L0 and late B, although their sample of stellar members with spectral types earlier than K6 ($M \gtrsim 1\,{\rm M}_{\odot}$) is relatively small. Meanwhile, for the much older population in the Upper Sco association ($t \sim 11$ Myr;

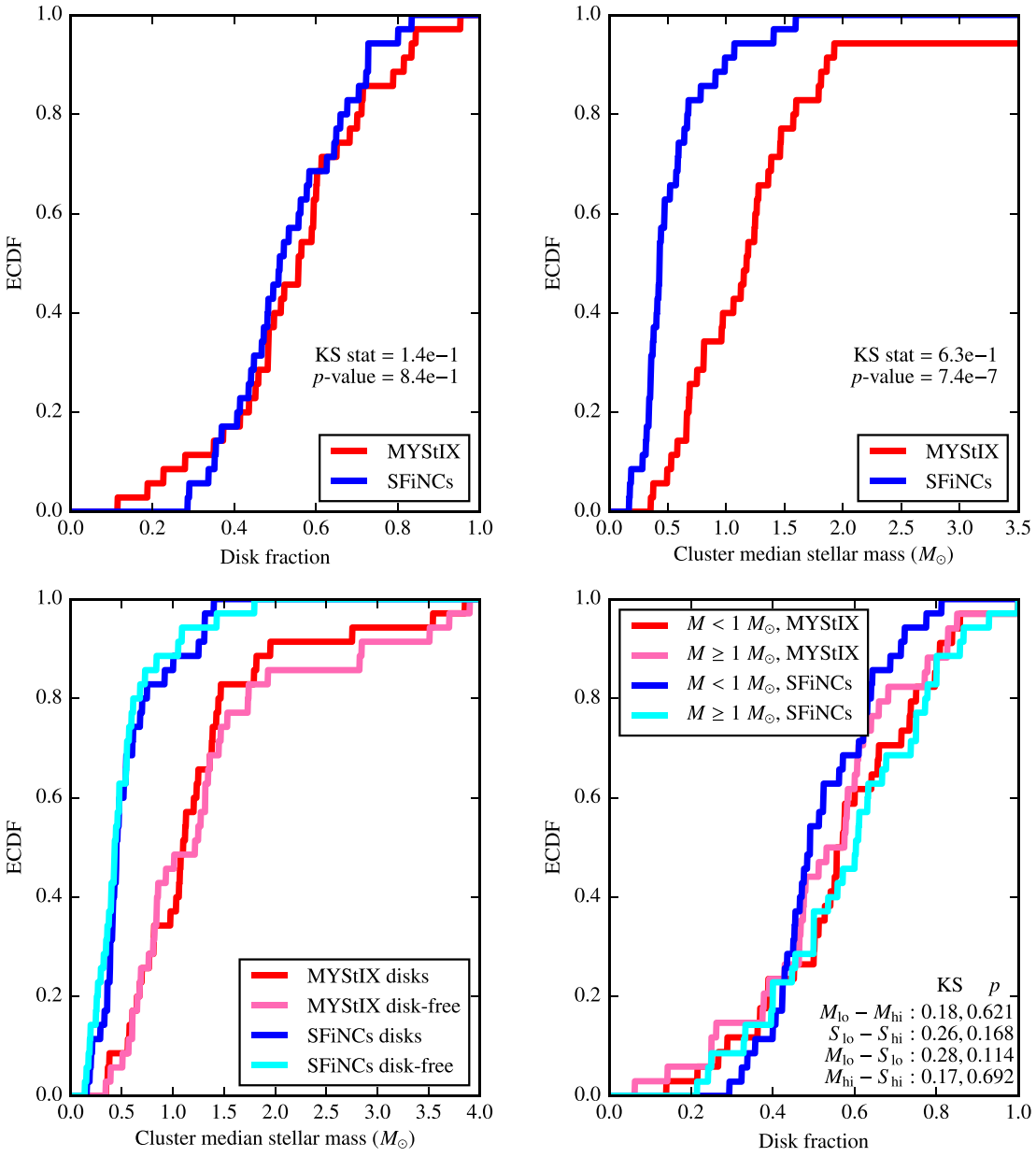

Figure 7. Cumulative distributions of cluster disc fraction (upper left panel), cluster median stellar mass (based on the Siess00 model; upper right panel), cluster median stellar mass separately for disc-bearing and disc-free YSOs (lower left panel), and disc fraction separately for low-mass ($M < 1$ M$_\odot$) and high-mass ($M \geq 1$ M$_\odot$) YSOs (lower right panel), separately for MYStIX and SFiNCs. The current figure shows a membership case with YSOs classified based on α_{IRAC} value and probable protostars included ($\alpha_{IRAC} > 0$). Figure panels showing cumulative distributions of disc fraction and median mass for the other three membership permutations are provided in the Supplementary Materials.

Pecaut et al. 2012), Luhman & Mamajek (2012) report a trend of a decreasing disc fraction from M-type to B–G type stars. These results may point to an increased disc depletion rate in higher mass stars throughout their disc evolution.

In Fig. 8, for the cases of catalogue-based YSO classification with and without probable protostars, we see diminished disc fractions for young (youngest two age bins), intermediate-mass (1–2 M$_\odot$) stars. To explore this, we first redo the analysis shown in Fig. 8 separately for MYStIX and SFiNCs (results not shown); the effect seems to emerge from the MYStIX sample alone. We also find that the increase in disc fraction going from the catalogue-based to the SED-based classifications comes from a gain in disc-bearing YSOs, not a loss of disc-free ones. Given the high nebulosity in many MYStIX regions, it is reasonable to suspect that contamination due to emission from polycyclic aromatic hydrocarbons (PAHs) reduces the sensitivity of YSO classification based on SED models towards disc-bearing YSOs. Indeed, we find that if we reproduce the analysis shown in Fig. 8 while excluding the three most heavily contaminated MYStIX clusters identified by Richert et al. (2015) based on 8 μm background levels, the effect in question disappears. This would seem to explain the large differences in M_{cut} between the catalogue YSO classifications and SED slope-based YSO classifications seen in Table 1, such as for NGC 6357 B, where the SED slope-based classifications achieve stellar mass completeness down to ∼0.1 M$_\odot$, as opposed to ∼0.6 M$_\odot$ for the catalogue classifications. X-ray measurements do not suffer from this problem, therefore the number

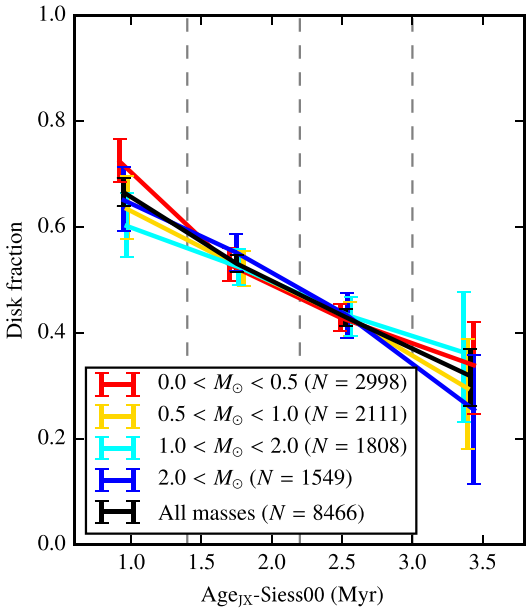

Figure 8. Disc fraction as a function of age (Age_{JX}-Siess00) for four bins of stellar mass, combining data across all 69 MYStIX and SFiNCs clusters. The current figure exhibits results for one of the four membership permutations, that is, the α_{IRAC}-based YSO classification with probable protostars included. Figure panels showing disc fraction as a function of age for the other three permutations (based on catalogue YSO classification with/without probable protostars included and based on the SED slope YSO classification when probable protostars are excluded) are provided in the Supplementary Materials. Vertical error bars are Wilson binomial confidence intervals for significance level 0.05. Dashed lines indicate age bin boundaries.

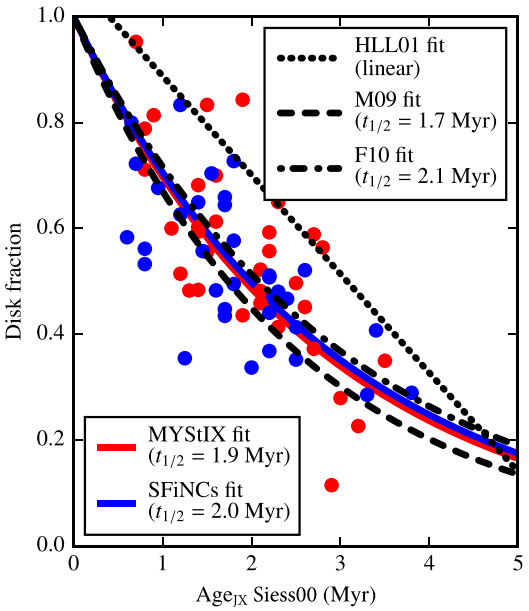

Figure 9. Disc fraction versus age (based on the Siess00 models) for 69 MYStIX and SFiNCs clusters, along with results of Haisch et al. (2001b, HLL01), Mamajek (2009, M09), and Fedele et al. (2010, F10). The MYStIX and SFiNCs fits are shown for the case of an SED slope-based YSO classification with probable protostars ($\alpha_{IRAC} > 0.0$) included.

of disc-free YSOs in the young-age, intermediate-mass regime in question does not change significantly between the catalog-based to SED-based classifications (Fig. 8).

Richert et al. (2015) find that in several distant, rich, OB-dominated MYStIX regions, the large point spread functions of early O stars in *Spitzer*/IRAC bands diminish sensitivity towards IRE from disc-bearing YSOs (whereas disc-free objects are still detected by X-rays). To ensure that the lower disc fraction for high-mass YSOs seen in Fig. 8 is not due to this effect, we perform the same analysis again, but now excluding OB-dominated regions identified as problematic by Richert et al. (2015), namely M 17 and NGC 6357. The results are not affected, apart from the effect discussed in the previous paragraph.

4 CONCLUSIONS

4.1 Summary of results

In this work, we have studied circumstellar disc longevity in 69 young stellar clusters by combining X-ray and infrared data and studying cluster disc fraction as a function of age. We have applied homogeneously derived cluster ages (based on the Age_{JX} method) and carefully accounted for the relative sensitivity to different clusters in the infrared and X-ray bands. The SFiNCs and MYStIX samples collectively exceed previous cluster samples by more than a factor of three.

Our data show that disc longevity estimates are strongly sensitive to the choice of PMS evolutionary model, but are not so sensitive to YSO classification scheme, initial disc fraction, stellar mass, and star-forming environment.

Our analysis has yielded IRAC half-lives of $t_{1/2} \sim 1.3$–2 Myr based on the non-magnetic Siess00 and MIST models, but much longer half-lives of $t_{1/2} \sim 3.5$ Myr based on the magnetic Feiden16M model. According to the relationship $\tau = t_{1/2}/ln(2)$, these half-lives $t_{1/2}$ translate into mean lifetimes of $\tau \sim 1.9$–2.9 Myr based on the non-magnetic Siess00 and MIST models, and $\tau \sim 5.0$ Myr based on the magnetic Feiden16M model.

Half-life estimates change only somewhat when the initial disc fraction is allowed to vary below 100 per cent, however the constraints on initial disc fraction and especially half-life are weak due to the limited age range of our sample.

We find no statistically significant evidence that disc fraction varies with stellar mass within the first few Myr of life. However, this result may be inaccurate for MYStIX and SFiNCs stars more massive than 2 $M_\odot$ due to reduced X-ray sensitivity towards mid-B and mid-A type stars.

Our data do not provide clear evidence that disc longevity depends on the surrounding star-forming environment.

4.2 Comparison with previous works

Our finding of a $t_{1/2} \sim 2$ Myr half-life (mean lifetime $\tau \sim 2.9$ Myr) for discs based on the Siess00 age scale agrees closely with those of several previous works (Mamajek 2009; Fedele et al. 2010; Ribas et al. 2014), which generally included heterogeneous compilations of cluster ages based on old-generation PMS evolutionary models. Fig. 9 shows a comparison of our results with those of Haisch et al. (2001b), Mamajek (2009), and Fedele et al. (2010). Our finding of a $t_{1/2} \sim 3.5$ Myr half-life (mean lifetime $\tau \sim 5.0$ Myr) based on the Feiden16M age scale is consistent with that of the recent work of Pecaut & Mamajek (2016). Detailed comparison with these studies follows.

(i) Haisch et al. (2001b). Fig. 9 shows that our disc fractions (based on the Siess00 model) are systematically lower than those of Haisch et al. (2001b, HLL01). One reason is differing disc classifications. The cluster IC 348 is found in both the SFiNCs and HLL01 samples, making it a useful example for exploring this possibility. In IC 348, ∼40 per cent of objects classified as disc-bearing by HLL01 are classified as disc-free in the SFiNCs catalogue. This indicates that the *JHKL*-based colour–colour diagram approach to identifying disc-bearing YSOs yields different results from those provided by longer wavelength (3–8 μm) data. A similar disparity in the disc classifications is provided by HLL01 and Lada et al. (2006), the latter of which makes use of *Spitzer* photometry; approximately a third of the YSOs shared between the HLL01 and Lada et al. (2006) catalogues have disparate classifications. Lada et al. (2006) notice that the $K-[3.6]$ colours of the stars in their work 'appear to be bluer than the $K-L$ colours of Haisch et al.', for unclear reasons. The SFiNCs *Spitzer*-IRAC photometric measurements are consistent with those of Lada et al. (see figure A3 in Getman et al. 2017). It is worth noting that our estimated disc fraction for IC 348 agrees closely with the estimate of Luhman et al. (2016). The level of 3.6 μm variability estimated by Flaherty et al. (2013) is small (standard deviations of order hundredths of a magnitude), and is therefore unlikely to lead to significant misclassification of YSOs.

A second possible explanation for the systematically higher disc fractions reported by HLL01 is related to their imposition of different mass limits for disc-bearing and disc-free objects as we discuss in Section 2.4. HLL01 use the analysis of Haisch et al. (2001a) to derive the disc fraction of IC 348. Haisch et al. (2001a) claim to be complete down to $L\sim12$ for disc-bearing and disc-free objects. However, in J and H bands, which trace the stellar photosphere and therefore serve as proxies for stellar mass, the sample of Haisch et al. (2001a) is substantially deeper for disc-bearing objects. L-band measurements are sensitive to the presence of a disc, therefore the imposition of a similar limit for disc-bearing and disc-free objects in the L band will be biased towards finding discs, leading to a significant overestimation of disc fraction. Excluding sources with $H>12$ for the Haisch et al. (2001a) catalogue in IC 348 lowers the disc fraction by a factor of ∼11 per cent. Correction for both effects (discrepancy in the $K-L$ colour and imposition of the L-band cuts) is needed to bring the HLL01 disc fraction in agreement with ours.

(ii) Mamajek (2009). He performs a literature compilation of heterogeneous sets of ages and disc fractions for 22 nearby young stellar clusters. His disc indicator is based on the combination of spectroscopic accretion and photometric IR excess signatures. Mamajek introduces the exponential decay formalism. For the compiled data set he obtains a mean-lifetime of $\tau=2.5$ Myr ($t_{1/2}=1.7$ Myr). MYStIX/SFiNCs Siess00-based disc dissipation time-scale of $t_{1/2}\sim2$ Myr is consistent with that of Mamajek despite the heterogeneity of Mamajeks' data set.

(iii) Fedele et al. (2010). They find that disc half-lives estimated based on spectroscopic indicators of accretion ($\tau=2.3$ Myr; $t_{1/2}=1.6$ Myr) are shorter than those based on IRE ($\tau=3.0$ Myr; $t_{1/2}=2.1$ Myr) to identify discs. The MYStIX/SFiNCs Siess00 result of $t_{1/2}\sim2$ Myr agrees with their estimate of disc lifetime based on IRE.

(iv) Pecaut et al. (2012) and Pecaut & Mamajek (2016). They find that for the Scorpius–Centaurus OB association, the age estimates of low-mass (K- and M-type) PMS stars are systematically lower (by a factor of two) compared to those of higher mass (G- and F-type) PMS and massive B-type main-sequence stars. This age discrepancy is likely related to the problem of 'radius inflation' in low-mass PMS stars (Section 1) and can be mitigated by introducing magnetic effects in PMS models (Somers & Pinsonneault 2015; Feiden 2016). For the Upper Sco (US), Upper Centaurus-Lupus (UCL), and Lower Centaurus-Crux (LCC) subregions of the OB association, Pecaut & Mamajek (2016) adopt HRD-based ages inferred for intermediate-mass G- and F-type PMS stars using the median age values among the output of four different, relatively modern PMS evolutionary models, including Dotter et al. (2008) and Baraffe15. Using these three clusters (US, UCL, and LCC), Pecaut & Mamajek (2016) estimate disc dispersal half-life of $t_{1/2}=3.3$ Myr ($\tau=4.7$ Myr).

The agreement with the MYStIX/SFiNCs half-life of $t_{1/2}\sim3.5$ Myr (based on the Feiden16M time-scale) is somewhat remarkable, considering the paucity of the Pecaut et al. cluster sample (only three clusters), as well as the following difference in disc indicators. As a disc indicator Pecaut & Mamajek (2016) use *WISE* photometry, which goes significantly farther into the infrared (3.4–22 μm), compared to *Spitzer*-IRAC employed by MYStIX/SFiNCs (3.6–8 μm). By probing cooler, farther-out regions of discs, we would expect the Pecaut et al. study to arrive at longer disc dispersal time-scales, but this has not occurred.

(v) Ribas et al. (2014). The last possibility discussed above is supported by disparate estimates of disc lifetimes for shorter wavelength (3.4–12 μm; $\tau\lesssim3$ Myr) and longer wavelength (22–24 μm; $\tau\gtrsim4$ Myr) observations (Ribas et al. 2014), reflecting differential evolution for different grain sizes and different regions of discs. Lada et al. (2006) classify several objects in IC 348 as disc-bearing that are designated as disc-free in the SFiNCs catalogue. Lada et al. (2006) use 24 μm *Spitzer* data to help identify discs, suggesting that the use of (<8 μm) infrared data as in the current work will fail to identify transition discs due to their lack of a hot inner component.

(vi) Bell et al. (2013). They introduce new semi-empirical model isochrones to correct the aforementioned problem of radius inflation and systematically lower ages for low-mass stars derived using standard PMS models (Pecaut et al. 2012; Pecaut & Mamajek 2016). Since a treatment of low-mass stellar ages is applied in Bell et al., we would expect to have our MYStIX/SFiNCs disc half-life of $t_{1/2}\sim3.5$ Myr (based on the Feiden16M time-scale), as well as that of Pecaut & Mamajek (2016), to be comparable with that of Bell et al. However, some complications arise.

For 13 clusters, Bell et al. combine their new age estimates with *Spitzer*-based disc fractions compiled from the literature to obtain a disc dissipation time-scale. Judging from their fig. 18, Bell et al. report a disc half-life of ∼5–6 Myr. Two issues arise here. First, Bell et al. do not provide any formal exponential fits to the data. By applying the non-linear Gauss–Newton least-squares method to fit an exponential function $f_{\rm disc}=f_0\times e^{t/\tau}$ (with $f_0=100$ per cent) to the data given in their fig. 18, we derive a disc half-life of $t_{1/2}\sim3$ Myr ($\tau\sim4.3$ Myr). This is rather inconsistent with their own reported value of ∼5–6 Myr.

Secondly, several regions are found in both the Bell et al. (2013) data set and the combined MYStIX and SFiNCs data set. These regions are Eagle Nebula, Lagoon Nebula, NGC 2264 (part of Rosette Nebula), IC 5146, Cep OB3b, and IC 348. Surprisingly, for the first four regions, these are Age_{JX}-Siess00 estimates and not *Age*-Feiden16M that appear to agree fairly well with those reported by Bell et al. (2013). MYStIX/SFiNCs *Age*-Feiden16M estimates are systematically higher than those of Bell et al.

For Cep OB3b and IC 348, our Age_{JX}-Siess00 and *Age*-Feiden16M ages are in the 2.5–4.5 Myr range, as opposed to the Bell et al. estimates of 6 Myr. While any number of factors affect age estimates, one partial explanation may be the disparate distance estimates between Bell et al. (2013) and the current work for Cep OB3b and IC 348, while the distance estimates agree more closely for the other

four regions. The ∼20 per cent disagreement in distances for these two clusters is likely a major factor in explaining the age disparity. Tycho-*Gaia* parallax distances for several objects in IC 348 confirm the SFiNCs adopted distance of 300 pc, as opposed to the distance of 250 pc adopted by Bell et al. (2013). As for Cep OB3b, Very Long Baseline Array parallax distances for two objects in Cep A – HW 2 and HW 9 – are ∼700 pc (Moscadelli et al. 2009; Dzib et al. 2011). Given the small (∼10 pc) projected distance between Cep A and Cep OB3b (Sargent 1977), we conclude that the Bell et al. (2013) distance of 570 pc based on CMDs is likely to be a substantial underestimation of the true distance. If the ages of Bell et al. (2013) for these two clusters are replaced with their Age_{JX}-Siess00 values from SFiNCs, the exponential half-life for the data shown in Bell et al. (2013) fig. 18 further decreases from $t_{1/2} \sim 3$ Myr to $t_{1/2} \sim 2$ Myr (assuming 100 per cent initial disc fraction). *Gaia* DR2 data will help to clarify these distance issues.

4.3 Suggestions for future work

To conclude, we distil the discussions of Sections 3 and 4 into suggestions for future studies of disc longevity.

(i) Large data sets using homogeneously derived cluster ages, based on PMS evolutionary models whose predictions are consistent with observations, are imperative for deriving reliable estimates of disc lifetimes and initial disc fraction. Our current work employing the largest cluster data set used in a study of this kind to date with homogeneous sets of cluster ages based on the old (Siess00) and modern (MIST, Feiden16M) sets of evolutionary models shows a strong effect of the choice of PMS models on the disc longevity estimates.

As discussed in Section 3.1.2, stronger constraints on disc lifetimes and initial disc fractions will require a sample that spans a range of stellar age longer than the characteristic time-scale of disc evolution. A larger age range will also allow for non-exponential parametrizations of the data to be explored. A significant sample of stars across all masses will be needed in order to resolve the question raised by our results in Section 3.3 of whether discs around high-mass stars evolve similarly to those orbiting lower mass stars.

(ii) Ensuring similar mass sensitivities for disc-bearing and disc-free sources is important for deriving reliable estimates of disc longevity and initial disc fraction, especially at older ages where disc fractions are low and subsequently sensitive to small differences in numbers of sources. Although we are concerned about this issue, it did not prove to be so important in other studies such as Mamajek (2009), Fedele et al. (2010), Ribas et al. (2014), and Pecaut & Mamajek (2016) except for HLL01. Since these previous studies focus mainly on nearby SFRs, it is possible that within the data sets employed, the disc-free and disc-bearing stellar samples have similar mass distributions.

The detection of disc-free YSOs will be greatly facilitated by the use of X-ray data, as well as the use of higher sensitivity infrared instruments such as those offered by the *James Webb Space Telescope*, especially for older objects with diminished X-ray luminosities. The imposition of consistent stellar mass sensitivity limits for disc-bearing and disc-free YSOs will be important for deriving strong constraints on disc lifetimes and initial disc frequencies, and also for exploring the role of stellar mass, cluster environment, and so on. Emission from PAHs in rich SFRs may pose a problem for ensuring consistent sensitivity towards disc-bearing and disc-free stars even for high-mass stars. Ensuring consistent sensitivity at higher masses may be important for calculating disc fractions among older systems (>3–5 Myr), where mass-dependent effects may emerge (based on the results of the current work, they do not seem to emerge for systems younger than a few Myr; however, our disc fractions inferred for $\gtrsim 2\,M_{\odot}$ stars may be overestimated due to the diminished X-ray sensitivity in mid-B and mid-A type stars).

(iii) Future studies of disc fraction versus age should separately explore multiple indicators of discs (while using otherwise homogeneous methods). In particular, using a large range of infrared through sub-mm wavelengths, as well as spectroscopic indicators, will help to determine how different regions of discs evolve. Near-/mid-infrared (1–8 μm) data are important for probing the inner several au of discs, providing constraints on the time available for the *in situ* formation of Earth analogs (though the presence of near-/mid-IRE does not necessarily indicate that a sufficient amount of dust for building a planet is available). Longer wavelength data, on the other hand, can provide insight into the evolution of the outer, cooler regions of discs, which appear to evolve more slowly (Ribas et al. 2014).

ACKNOWLEDGEMENTS

We thank the referee for his/her very helpful comments. We thank K. Luhman, E. Mamajek, M. Pecaut, G. Somers, and R. Jeffries for stimulating discussions. The MYStIX project is now supported by the *Chandra* archive grant AR7-18002X. The SFiNCs project is supported at Penn State by NASA grant NNX15AF42G, *Chandra* GO grant SAO AR5-16001X, *Chandra* GO grant GO2-13012X, *Chandra* GO grant GO3-14004X, *Chandra* GO grant GO4-15013X, and the *Chandra* ACIS Team contract SV474018 (G. Garmire and L. Townsley, Principal Investigators), issued by the *Chandra* X-ray Center, which is operated by the Smithsonian Astrophysical Observatory for and on behalf of NASA under contract NAS8-03060. The Guaranteed Time Observations (GTO) data used here were selected by the ACIS Instrument Principal Investigator, Gordon P. Garmire, of the Huntingdon Institute for X-ray Astronomy, LLC, which is under contract to the Smithsonian Astrophysical Observatory; Contract SV2-82024. This research has made use of NASA's Astrophysics Data System Bibliographic Services and SAOImage DS9 software developed by Smithsonian Astrophysical Observatory.

REFERENCES

Alencar S. H. P. et al., 2010, A&A, 519, A88
Anderson K. R., Adams F. C., Calvet N., 2013, ApJ, 774, 9
Armitage P. J., 2011, ARA&A, 49, 195
Audard M. et al., 2014, in Beuther H., Klessen R. S., Dullemond C. P., Henning T., eds, Protostars and Planets VI. Univ. Arizona Press, Tucson, AZ, p. 387
Bai X.-N., 2011, ApJ, 739, 50
Baraffe I., Chabrier G., Allard F., Hauschildt P. H., 1998, A&A, 337, 403
Baraffe I., Homeier D., Allard F., Chabrier G., 2015, A&A, 577, A42 (Baraffe15)
Bell K. R., Cassen P. M., Klahr H. H., Henning T., 1997, ApJ, 486, 372
Bell C. P. M., Naylor T., Mayne N. J., Jeffries R. D., Littlefair S. P., 2013, MNRAS, 434, 806
Boss A. P., 2010, in Bulletin of American Astronomical Society, Vol. 42, AAS/Division for Planetary Sciences Meeting Abstracts #42. p. 1070
Bouvier J., Cabrit S., Fernandez M., Martin E. L., Matthews J. M., 1993, A&A, 272, 176
Bressan A., Marigo P., Girardi L., Salasnich B., Dal Cero C., Rubele S., Nanni A., 2012, MNRAS, 427, 127
Broos P. S. et al., 2013, ApJS, 209, 32
Brown L. D., Cai T. T., DasGupta A., 2001, Stat. Sci., 16, 101
Carpenter J. M., Mamajek E. E., Hillenbrand L. A., Meyer M. R., 2006, ApJ, 651, L49

Castelli F., Kurucz R. L., 2004, preprint (arXiv: astro-ph/0405087)
Choi J., Dotter A., Conroy C., Cantiello M., Paxton B., Johnson B. D., 2016, ApJ, 823, 102 (MIST)
Cody A. M. et al., 2014, AJ, 147, 82
Cloutier R., Currie T., Rieke G. H., Kenyon S. J., Balog Z., Jayawardhana R., 2014, ApJ, 796, 127
Dennis Jr J. E., Gay D. M., Walsh R. E., 1981, ACM Trans. Math. Softw., 7, 348
Dotter A., 2016, ApJS, 222, 8
Dotter A., Chaboyer B., Jevremović D., Kostov V., Baron E., Ferguson J. W., 2008, ApJS, 178, 89
Drake J. J., Braithwaite J., Kashyap V., Günther H. M., Wright N. J., 2014, ApJ, 786, 136
Dzib S., Loinard L., Rodríguez L. F., Mioduszewski A. J., Torres R. M., 2011, ApJ, 733, 71
Fang Q., Herczeg G. J., Rizzuto A., 2017, ApJ, 842, 123
Fedele D., van den Ancker M. E., Henning T., Jayawardhana R., Oliveira J. M., 2010, A&A, 510, A72 (F10)
Feiden G. A., 2016, A&A, 593, A99 (Feiden16)
Feiden G. A., Jones J., Chaboyer B., 2015, in van Belle G. T., Harris H. C., eds, 18th Cambridge Workshop on Cool Stars, Stellar Systems, and the Sun, Vol. 18, Lowell Observatory, p. 171
Feigelson E. D. et al., 2013, ApJS, 209, 26
Flaherty K. M., Muzerolle J., Rieke G., Gutermuth R., Balog Z., Herbst W., Megeath S. T., 2013, AJ, 145, 66
Getman K. V., Feigelson E. D., Sicilia-Aguilar A., Broos P. S., Kuhn M. A., Garmire G. P., 2012, MNRAS, 426, 2917
Getman K. V. et al., 2014, ApJ, 787, 108
Getman K. V., Broos P. S., Kuhn M. A., Feigelson E. D., Richert A. J. W., Ota Y., Bate M. R., Garmire G. P., 2017, ApJS, 229, 28
Getman K. V., Kuhn M. A., Feigelson E. D., Broos P. S., Bate M. R., Garmire G. P., 2018, MNRAS, 477, 298
Güdel M., Nazé Y., 2009, A&AR, 17, 309
Güdel M. et al., 2007, A&A, 468, 353
Gutermuth R. A., Megeath S. T., Myers P. C., Allen L. E., Pipher J. L., Fazio G. G., 2009, ApJS, 184, 18
Haisch K. E., Jr, Lada E. A., Lada C. J., 2001a, AJ, 121, 2065
Haisch K. E., Jr, Lada E. A., Lada C. J., 2001b, ApJ, 553, L153 (HLL01)
Hernández J., Calvet N., Hartmann L., Briceño C., Sicilia-Aguilar A., Berlind P., 2005, AJ, 129, 856
Hernández J., Hartmann L., Calvet N., Jeffries R. D., Gutermuth R., Muzerolle J., Stauffer J., 2008, ApJ, 686, 1195
Hernández J., Morales-Calderon M., Calvet N., Hartmann L., Muzerolle J., Gutermuth R., Luhman K. L., Stauffer J., 2010, ApJ, 722, 1226
Jeffries R. D., 2017, Mem. Soc. Astron. Ital., 88, 637
Jeffries R. D. et al., 2017, MNRAS, 464, 1456
Kennedy G. M., Kenyon S. J., 2009, ApJ, 695, 1210
Königl A., Salmeron R., 2011, in Garcia P. J. V., ed., Physical Processes in Circumstellar Disks around Young Stars. Univ. Chicago Press, Chicago, IL, p. 283
Kraus A. L., Cody A. M., Covey K. R., Rizzuto A. C., Mann A. W., Ireland M. J., 2015, ApJ, 807, 3
Kuhn M. A., Getman K. V., Feigelson E. D., Reipurth B., Rodney S. A., Garmire G. P., 2010, ApJ, 725, 2485
Kuhn M. A., Getman K. V., Broos P. S., Townsley L. K., Feigelson E. D., 2013a, ApJS, 209, 27
Kuhn M. A., Povich M. S., Luhman K. L., Getman K. V., Busk H. A., Feigelson E. D., 2013b, ApJS, 209, 29
Kuhn M. A. et al., 2014, ApJ, 787, 107
Kuhn M. A., Getman K. V., Feigelson E. D., 2015a, ApJ, 802, 60
Kuhn M. A., Feigelson E. D., Getman K. V., Sills A., Bate M. R., Borissova J., 2015b, ApJ, 812, 131
Lada C. J. et al., 2006, AJ, 131, 1574
Luhman K. L., Mamajek E. E., 2012, ApJ, 758, 31
Luhman K. L., Esplin T. L., Loutrel N. P., 2016, ApJ, 827, 52 (Lu16)
Lynden-Bell D., Pringle J. E., 1974, MNRAS, 168, 603
Lyra W., Johansen A., Klahr H., Piskunov N., 2008, A&A, 491, L41
Mamajek E. E., 2009, in Usuda T., Tamura M., Ishii M., eds, AIP Conf. Proc. Vol. 1158, Exoplanets and Disks: Their Formation and Diversity. Am. Inst. Phys., New York, p. 3 (M09)
Moscadelli L., Reid M. J., Menten K. M., Brunthaler A., Zheng X. W., Xu Y., 2009, ApJ, 693, 406
Naylor T., Broos P. S., Feigelson E. D., 2013, ApJS, 209, 30
Pecaut M. J., Mamajek E. E., 2016, MNRAS, 461, 794
Pecaut M. J., Mamajek E. E., Bubar E. J., 2012, ApJ, 746, 154
Portegies Zwart S. F., 2016, MNRAS, 457, 313
Povich M. S. et al., 2013, ApJS, 209, 31
Preibisch T., 2012, Res. Astron. Astrophys., 12, 1
Pringle J. E., 1981, ARA&A, 19, 137
R Core Team 2014, R: A Language and Environment for Statistical Computing. R Foundation for Statistical Computing, Vienna, Austria, http://www.R-project.org/
Ribas Á., Merín B., Bouy H., Maud L. T., 2014, A&A, 561, A54
Ribas Á., Bouy H., Merín B., 2015, A&A, 576, A52
Richert A. J. W., Feigelson E. D., Getman K. V., Kuhn M. A., 2015, ApJ, 811, 10
Rieke G. H., Lebofsky M. J., 1985, ApJ, 288, 618
Robitaille T. P., Whitney B. A., Indebetouw R., Wood K., Denzmore P., 2006, ApJS, 167, 256
Sargent A. I., 1977, ApJ, 218, 736
Shakura N. I., Sunyaev R. A., 1973, A&A, 24, 337
Siess L., Dufour E., Forestini M., 2000, A&A, 358, 593 (Siess00)
Soderblom D. R., Hillenbrand L. A., Jeffries R. D., Mamajek E. E., Naylor T., 2014, in Beuther H., Klessen R. S., Dullemond C. P., Henning T., eds, Protostars and Planets VI. Univ. Arizona Press, Tucson, AZ, p. 219
Somers G., Pinsonneault M. H., 2015, ApJ, 807, 174
Somers G., Stassun K. G., 2017, AJ, 153, 101
Stelzer B., Robrade J., Schmitt J. H. M. M., Bouvier J., 2009, A&A, 493, 1109
Strom K. M., Strom S. E., Edwards S., Cabrit S., Skrutskie M. F., 1989, AJ, 97, 1451
Telleschi A., Güdel M., Briggs K. R., Audard M., Palla F., 2007, A&A, 468, 425
Townsley L. K., Broos P. S., Garmire G. P., Bouwman J., Povich M. S., Feigelson E. D., Getman K. V., Kuhn M. A., 2014, ApJS, 213, 1
Vincke K., Pfalzner S., 2016, ApJ, 828, 48
Wilson E. B., 1927, J. Am. Stat. Assoc., 22, 209
Youdin A. N., Goodman J., 2005, ApJ, 620, 459

SUPPORTING INFORMATION

Supplementary data are available at *MNRAS* online.

Figure 4. Disc fraction versus Age_{JX}-Siess00 for 69 MYStIX and SFiNCs clusters (red and blue points, respectively).
Figure 5. Disc fraction as a function of age using three types of cluster ages (Age_{JX}-Siess00, Age_{JX}-MIST, and *Age*-Feiden16M).
Figure 7. Cumulative distributions of cluster disc fraction (upper left panel), cluster median stellar mass (based on the Siess00 model; upper right panel), cluster median stellar mass separately for disc-bearing and disc-free YSOs (lower left panel), and disc fraction separately for low-mass ($M < 1$ M$_\odot$) and high-mass ($M \geq 1$ M$_\odot$) YSOs (lower right panel), separately for MYStIX and SFiNCs.
Figure 8. Disc fraction as a function of age (Age_{JX}-Siess00) for four bins of stellar mass, combining data across all 69 MYStIX and SFiNCs clusters.
Table 1. Properties of 69 MYStIX and SFiNCs clusters.

Please note: Oxford University Press is not responsible for the content or functionality of any supporting materials supplied by the authors. Any queries (other than missing material) should be directed to the corresponding author for the article.

This paper has been typeset from a TEX/LATEX file prepared by the author.